Gondwana Research 103 (2022) 335–361

Contents lists available at ScienceDirect

Gondwana Research

journal homepage: www.elsevier.com/locate/gr

Paleogeography of the West Burma Block and the eastern Neotethys Ocean: Constraints from Cenozoic sediments shed onto the Andaman-Nicobar ophiolites

Pinaki C. Bandopadhyay [a,1], Douwe J.J. van Hinsbergen [b,*], Debaditya Bandyopadhyay [a,c,d], Alexis Licht [e,f], Eldert L. Advokaat [b,g], Alexis Plunder [b,h], Biswajit Ghosh [a], Arnab Dasgupta [i], João P. Trabucho-Alexandre [b]

[a] Department of Geology, University of Calcutta, 35 Ballygunge Circular Road, Kolkata 700019, India
[b] Department of Earth Sciences, Utrecht University, Princetonlaan 8A, 3584 CB Utrecht, the Netherlands
[c] Department of Geology, University of North Bengal, Darjeeling 734013, India
[d] Earthquake Research Institute, The University of Tokyo, Tokyo 113-0032, Japan
[e] Department of Earth and Space Sciences, University of Washington, Seattle, WA, USA
[f] Aix-Marseille Université, CNRS, Centre de Recherche et d'Enseignement de Géosciences de l'Environnement (CEREGE), Aix-en-Provence, France
[g] School of Geography, Earth and Environmental Sciences, University of Birmingham, B15 2TT, UK
[h] BRGM, F-45060 Orléans, France
[i] Department of Geology, Government General Degree College, Manbazar-II, Susunia, Purulia 723131, India

ARTICLE INFO

Article history:
Received 2 April 2021
Revised 8 October 2021
Accepted 20 October 2021
Available online 26 October 2021
Handling Editor: I. Somerville

Keywords:
Neotethys Ocean
Paleogeography
Sediment provenance
Forearc
Collision

ABSTRACT

The Andaman and Nicobar ophiolites, in the forearc of the western Sunda subduction zone, underwent enigmatic, rapid Cenozoic vertical motions: shallow-water sediments with abundant arc debris characterize the middle Paleocene–middle Eocene and are under- and overlain by significantly deeper sediments. Recent paleomagnetic results revealed a near-equatorial paleolatitude of the West Burma Block and the associated subduction zone, at a similar latitude as the Andaman forearc until the early Eocene, providing a new avenue toward explaining the unusual stratigraphy. Here, we studied the provenance of the clastic sediments of the Andaman-Nicobar accretionary ridge using petrography, geochemistry, and detrital zircon geochronology. We found that the Paleocene-Eocene Namunagarh Grit is likely to be derived from a then proximal, 60 Ma old arc that was likely located in the ocean to the north (present-day east) of the West Burma Block, west of Andaman-Nicobar. The Oligocene–lower Miocene East Andaman Flysch contains West Burma Block debris that traveled much farther and mixed with sediments derived from Sundaland. The West Andaman and Great Nicobar Flysch have an additional Himalayan source consistent with derivation from the downgoing plate. We interpret this history as reflecting the late Paleocene–early Eocene collision of the West Burma Block, likely then part of the Australian Plate, with the Andaman forearc causing uplift and proximal sedimentation shed from the colliding arc. Subsequent northward motion of the West Burma Block caused subsidence of the Andaman forarc and N-S opening of the Andaman Sea, which opened a pathway for Sundaland-derived sediments to reach the Andaman ophiolites. The recently proposed high Cenozoic mobility of the West Burma Block remains to be reconciled in detail with geological observations in Myanmar and Sundaland, but our results show that this scenario provides ample opportunity to explain the previously enigmatic stratigraphic evolution of the Andaman and Nicobar Islands.

1. Introduction

Plate kinematic and paleogeographic reconstructions based on geological observations form the basis for the analysis of mantle dynamics, paleoclimate, paleoceanography, and paleobiology (e.g., Scotese, 2004). Whereas reconstructions of the modern oceans are relatively straightforward and restore the

* Corresponding author.
E-mail address: d.j.j.vanhinsbergen@uu.nl (D.J.J. van Hinsbergen).
[1] Present Address: 40, Bajeshibpur Road, Howrah-2, WB, India.

https://doi.org/10.1016/j.gr.2021.10.011
1751-7311/

paleogeographic evolution of the major continents back to the times of Pangea (e.g., Müller et al., 2016; Seton et al., 2012), restoring the paleogeography and plate boundary evolution of now-subducted lithosphere is more challenging. Such reconstructions rely on geological and geophysical analysis of incomplete and highly deformed fragments of crust preserved in accretionary orogens and collision zones (e.g., Scotese, 2004; Stampfli and Borel, 2002; Torsvik and Cocks, 2017; van Hinsbergen and Schouten, 2021; van Hinsbergen et al., 2020). But interpretations of these accreted geological records often conflict, leading to debate, as exemplified by the paleogeography of the lithosphere of the eastern Neotethyan realm that was subducted between India-Australia and Eurasia.

Restoring eastern Neotethys paleogeography that was consumed by subduction accommodating convergence between the Indian and Australian plates, and Eurasia relies on the relative positions of India, Australia, and Eurasia constrained from plate circuits (e.g., Patriat and Achache, 1984; Seton et al., 2012; van Hinsbergen et al., 2011b), and by using the oceanic and continental rocks accreted to the Himalayan and SE Asian orogens (e.g., Hall, 2012; Metcalfe, 2013; Westerweel et al., 2019). Combined, these lead to reconstructions of the ocean-continent distribution, land-sea distribution, and plate boundary configuration of the now-subducted lithosphere through time. Key constraints to determine paleogeography come from, for example, the timing of collision or breakup using the onset or arrest of sediment exchange between two blocks, paleomagnetic data constraining paleolatitude and rotation of blocks, and timing and style of deformation, metamorphism, and magmatism (e.g., Hu et al., 2016; Kapp and DeCelles, 2019; van Hinsbergen et al., 2019; Westerweel et al., 2019). These datasets have led to the consensus that a long-lived subduction zone existed from Early Cretaceous or earlier time along the southern Eurasian margin of Tibet that continuously or intermittently consumed oceanic crust of the eastern Neotethys Ocean, until the arrival of continental rocks of the Indian plate preserved in the northern, Tibetan Himalaya (Hu et al., 2016; Kapp and DeCelles, 2019; van Hinsbergen et al., 2019). In addition, paleomagnetic and seismic tomographic arguments have been brought forward to advocate that also intra-oceanic subduction zones may have existed within the Neotethys (Aitchison et al., 2007; Jagoutz et al., 2015; Martin et al., 2020; Parsons et al., 2020; Tapponnier et al., 1981; Westerweel et al., 2019). Multiple subduction zones may make the plate kinematic construction more complex and have led to the interpretation of additional plates that converged with India-Australia as well as Eurasia (Jagoutz et al., 2015; Tapponnier et al., 1981; Westerweel et al., 2019). Of particular interest in the paleogeographic debate of the eastern Neotethys is the West Burma Block that occupies much of Myanmar today: this block was long considered part of Eurasia since Mesozoic time (e.g., Barber and Crow, 2009; Hall, 2012; Sevastjanova et al., 2016), but U–Pb detrital zircon geochronology (Yao et al., 2017; Zhang et al., 2020) suggested the block was located near the NW Australian margin in the Late Triassic, and paleomagnetic data suggest that the block was at equatorial latitudes from the Cretaceous until the late Eocene and gradually moved northward since (Westerweel et al., 2019; 2020). Together with geological constraints from Sumatra and the Andaman Islands, which appear to have been above a subduction zone since the Cretaceous (Bandyopadhyay et al., 2021; Barber et al., 2005; Plunder et al., 2020), this suggests that the West Burma Block occupied an intra-oceanic position, on a separate plate from Eurasia until as recent as the Eocene (Westerweel et al., 2019). Paleomagnetic data, however, only provide paleolatitudinal control, and the paleolongitudinal position or motion of the West Burma Block remains unconstrained.

A key new constraint to this end may come from sedimentary rocks that are exposed on the Andaman Islands that lie in the Indian Ocean to the south of the West Burma Block. There, a series of upper Paleocene–Eocene shallow-water volcaniclastic sedimentary rocks and Oligo-Miocene deepwater siliciclastic turbiditic sequences overlie and structurally underlie Cretaceous ophiolites and associated pelagic sediments. The Cenozoic sediments have previously been interpreted and reconstructed under the assumption that the West Burma Block had been located to the north of the Andaman Islands since the Cretaceous and in the forearc of the Sunda subduction zone. In this context, clastic sedimentary deposits on the Andaman Islands were either interpreted as coming from Myanmar (Allen et al., 2008), from India (Limonta et al., 2017), or both (Awasthi, 2017). Tectonic reconstructions restoring the N-S opening of the Andaman Sea, between the Andaman Islands, West Burma, Sumatra, and mainland Sundaland (Curray, 2005; Morley, 2017), reveal that the West Burma Block was in early Oligocene time located immediately north of Sumatra, and the Andaman Islands just northwest of Sumatra, in the forearc of the Sunda subduction zone (Advokaat et al., 2018a; Morley and Arboit, 2019). The sedimentary geological evolution of the Andaman Islands has thus been interpreted in terms of the northward translation of the West Burma Block away from Sumatra, in the forearc of the subducting oceanic Indian plate. But it has remained puzzling what may have caused the strong vertical motions recorded by the Cenozoic Andaman sedimentary record, and how clastic sediments from the hinterland would have reached the Andaman Islands. The new paleomagnetic constraints from (Westerweel et al., 2019; 2020) invite a re-evaluation of the paleogeography of the West Burma Block relative to Sundaland using the Andaman sedimentary record, which we attempt in this paper. To this end, we provide new petrographic and detrital zircon U-Pb data from the Paleocene to Miocene sedimentary record of the Andaman Islands. We evaluate and integrate previous and new data and compare this with regional sources to decipher the Paleogene sediment pathways along the Sunda margin and discuss these in the light of eastern Neotethyan paleogeography.

2. Geological setting

2.1. Regional setting

The Andaman-Nicobar Archipelago is an outer arc-forearc high located immediately east of the Sunda subduction zone. The Cretaceous Andaman Ophiolites (Bandyopadhyay et al., 2021; Pedersen et al., 2010; Sarma et al., 2010), are part of a sliver plate that also includes the West Burma Block to the north. This sliver plate is bounded from India by an east-dipping subduction zone, and from Sundaland, including eastern Sumatra, by a dextral transform system (Fig. 1). The N-S extensional, Andaman Sea forms an extensional step-over on this transform system and connects the Sagaing fault in the NE to the West Andaman Fault in the SW, which branches into several faults, including the active Sumatra Fault System, that connect in triple junctions to the Sunda Trench (Curray, 2005; Huchon and Le Pichon, 1984; Lelgemann et al., 2000; Sieh and Natawidjaja, 2000). Stratigraphic records in basins along the Sagaing fault and Andaman Sea, and cooling ages of exhumed basement rocks along the Shan Scarp reveal that this sliver plate has existed since the mid-Oligocene, ~28 Ma (Bertrand et al., 1999; 2001; Bertrand and Rangin, 2003; Arboit and Morley, 2019; Lamont et al., 2021). Tectonic reconstruction of the Andaman Sea and western Sundaland suggests that in that time, the West Burma-Andaman sliver plate moved some 800–1000 km northward relative to Sumatra (van Hinsbergen et al., 2011a), consistent with recent paleomagnetic constraints of the West Burma Block (Westerweel et al., 2020). Restoring this motion would bring the Andaman Ophiolites adjacent to, and in the forearc

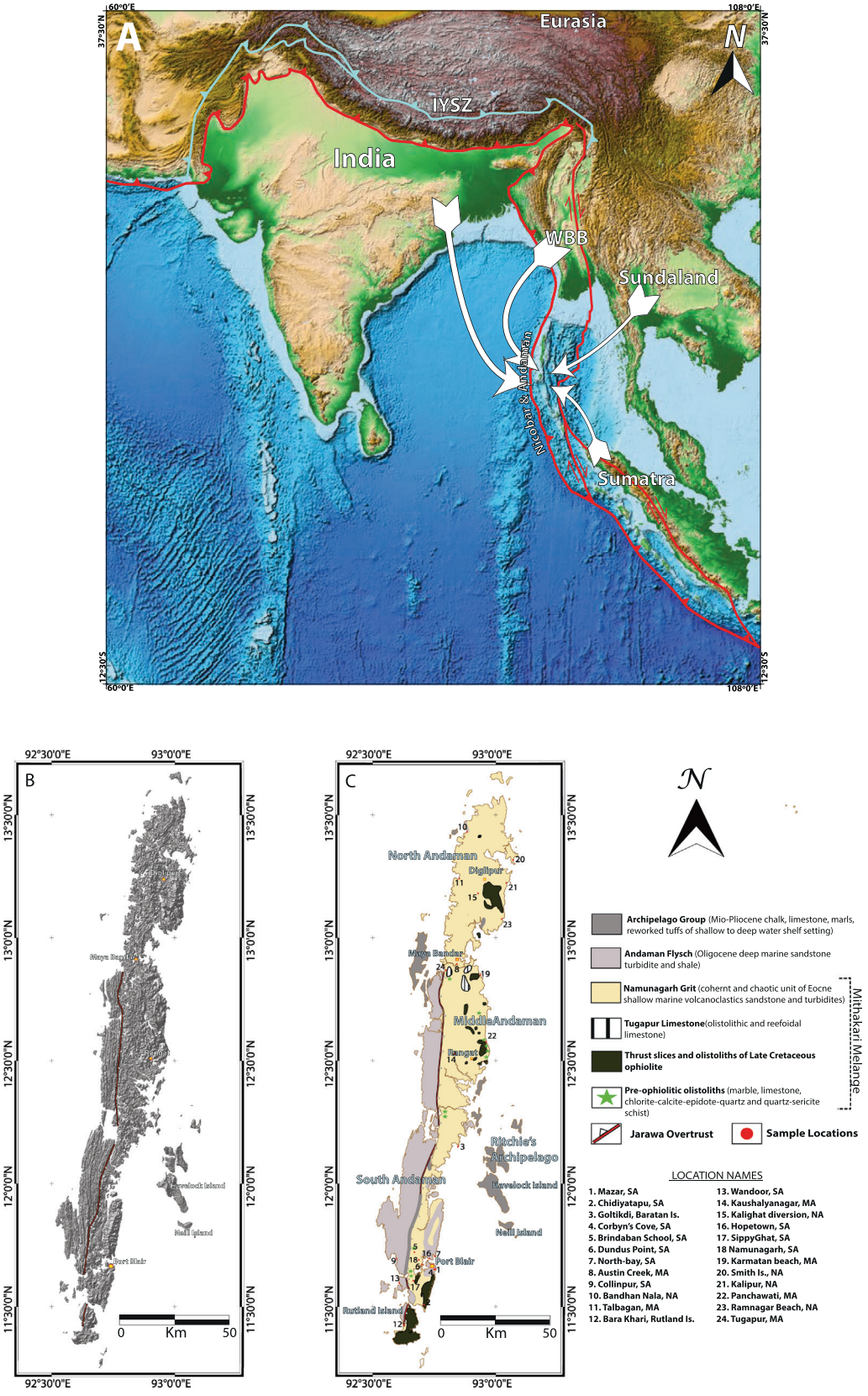

Fig. 1. A) Location of the Andaman-Nicobar accretionary ridge within the tectonic framework of Western Sunda Arc, SE Asia. B) Digital elevation image of the Andaman Islands depicting two N-S trending terranes (coherent and chaotic) with distinct geomorphic and topographic expression. Parallel ridges and steep valley characterize the coherent terrane extended all along the western side and mapped as Andaman Flysch Formation whereas the eastern side depicts chaotic occurrences of discrete and moderate and high-relief hills mapped as ophiolites, hillocks of trench sediments (Namunagarh Grit), and low-lying coastal planes strewn with boulders and blocks of melange rocks. C) Outline geological map of Andaman showing field setting of different tectono-stratigraphic units and the N-S structural grain of the islands almost parallel to Sunda trench (for locations see Table 1).

of northwestern Sumatra in Oligocene time and juxtaposes the southern West Burma Block against northern Sumatra (Advokaat et al., 2018a).

The geology of Sumatra and West Burma is markedly different, suggesting that the Andaman Sea reactivates an older tectonic boundary that juxtaposed the two. Sumatra hosts the Woyla Arc (Barber, 2000; Barber and Crow, 2009; Wajzer et al., 1991), which formed in an intra-oceanic position in Early Cretaceous time and collided with and accreted to continental Sundaland in the mid-Cretaceous, around 105–95 Ma (Advokaat et al., 2018a; Barber et al., 2005). Subduction between the Woyla Arc and Sundaland ceased in that period, but convergence of India or Australia with Sundaland continued. The Andaman Ophiolites have a metamorphic sole that was cooling by ~105 Ma (Plunder et al., 2020) and the ophiolites have a geochemistry that suggests that crust originally formed in a back-arc basin environment became overprinted by spreading in a forearc basin by that time, and on which a more mature volcanic arc started forming by 98–93 Ma (Bandyopadhyay et al., 2021). It is thus feasible that the Andaman ophiolites recorded the subduction initiation along the western margin of the Woyla Arc that followed upon arrest of subduction between the Woyla Arc and Sundaland (Advokaat et al., 2018a; Bandyopadhyay et al., 2021; Plunder et al., 2020), which places the record of the Andaman Islands in the Sundaland forearc since at least 105 Ma.

To the north of the Andaman Sea, the West Burma Block (Fig. 1A) contains Paleozoic metasediments with an Australian provenance (Aitchison et al., 2019) that hosts a long-lived volcanic arc, the Wuntho-Popa Arc, that has existed since the Early Cretaceous (Li et al., 2019; Licht et al., 2020; Than et al., 2017; Wang et al., 2014). This arc is likely associated with a west-verging belt of forearc ophiolites with ages of 133–115 Ma that fringes the West Burma Block in the west (Liu et al., 2016; Singh et al., 2017; Zhang et al., 2018; Aitchison et al., 2019). Below these ophiolites is an accretionary fold-thrust belt that includes Ocean Plate Stratigraphy of Late Triassic to Early Cretaceous age (Baxter et al., 2011; Zhang et al., 2018; Aitchison et al., 2019; Rajkakati et al., 2019), and the continent-derived Mount Victoria Block that hosts Triassic sediments, also with an Australian provenance (Yao et al., 2017; Zhang et al., 2020) that accreted to the West Burma Block around 115 Ma (Zhang et al., 2017; 2018; Morley et al., 2020). The West Burma Block represents a Gondwana-derived continental fragment that has been in the upper plate of a subduction zone since the Early Cretaceous, in which Triassic and younger oceanic crust, as well as other Gondwana-derived slivers, were consumed. The paleomagnetic data of Westerweel et al. (2019; 2020) suggest that this subduction zone was located at the same latitude as Sumatra and, by inference, the Andaman Islands, which, if true, implies that the Myanmar and Andaman subduction zones were not the same. Westerweel et al. (2019) proposed a Burma-Sundaland collision sometime during the Paleogene, likely along or south of the Andaman subduction zone. By contrast, Morley et al. (2020) and Westerweel et al. (2020) proposed that the West Burma Block remained outboard the Andaman and Sumatra Trench during most of the Paleogene, separated by a transform system merging into the eastern Himalayan syntaxis; the west Burma Block would have accreted to the Sundaland margin later, in the late Oligocene. Regardless of the chronology of accretion between Burma and Sundaland, the West Burma Block must have arrived in a N-S oriented position north of Sumatra by early Oligocene time at the latest, from where it took its northward flight as a sliver plate, together with the Andaman Ophiolites. Both scenarios require a suture between the West Burma Block and Sundaland to be located somewhere in the Andaman Sea (Morley et al., 2021).

2.2. Geology of the Andaman Islands

The Andaman-Nicobar archipelago in the Northeast Indian Ocean stretches for ~700 km in a north–south direction and exposes the non-volcanic forearc known as the Andaman-Nicobar Ridge adjacent to the Sunda trench that represents the active subduction zone of the Indo-Australian plate below the West Burma sliver plate (Roy, 1992). On the downgoing Indo-Australian plate to the west of the Sunda trench are the voluminous Bengal and Nicobar submarine fans, divided by the Ninety-East Ridge, a volcanic seamount chain. Recent work revealed that the Nicobar fan contains distal turbidites with ages dating back to at least 19 Ma, and with a Tibetan provenance, drained by the Brahmaputra River (Mcneill et al., 2017; Chen et al., 2020; Pickering et al., 2020).

The Andaman and Nicobar archipelago is extensively covered by tropical forest, thus geologic exposures/outcrops on the islands are restricted to road cuts, streams, and (particularly the eastern) coastal exposure. Despite these limited exposures, a stratigraphy of the island has been established (Fig. 2). The Upper Cretaceous ophiolites, presumably the basement of the Paleogene-Neogene sedimentary succession, retained back-arc basin, supra-subduction zone, and arc geochemical signatures (Bandyopadhyay et al., 2020; 2021; Ghosh et al., 2009; Pal, 2011). Below the Andaman Ophiolites lies a metamorphic sole that represents the highest part of the accretionary prism (Pal and Bhattacharya, 2010; Plunder et al., 2020). The oldest ages of the ophiolites coincide with 105 Ma $^{40}Ar/^{39}Ar$ cooling ages from the metamorphic sole, and likely represent the supra-subduction zone spreading stage (Bandyopadhyay et al., 2021; Plunder et al., 2020), which followed subduction initiation in a back-arc basin environment, likely behind the Woyla Arc (Bandyopadhyay et al., 2021). Maturation of the arc is reflected by 98–93 Ma plagiogranites and gabbros with arc geochemical signatures (Bandyopadhyay et al., 2021; Sarma et al., 2010; Pedersen et al., 2010). The ophiolite and sole are underlain by a serpentinite and sediment-hosted mélange that contains metamorphic sole fragments as well as radiolarian cherts with ages up to Eocene (Pal and Bhattacharya, 2010; Plunder et al., 2020). The ophiolites and overlying sediments are bound in the west by the prominent Jarawa Thrust that is traced all along the Andaman Islands. Satellite image (Fig. 1B) and geological map (Fig. 1C) clearly display that the east and west of the Jarawa Thrust have markedly different geology, topography and geomorphology. Deep-marine turbidites to the west of the Jarawa Thrust are most likely part of a basin scale deposit of an active margin, (siliciclastic) sand-rich submarine fan, while ophiolites, mélanges, Namunagarh Grit, and pelagic sediments to the east of the Jarawa Thrust are accretionary prism rocks, as evident from the interbedded turbiditic sandstones and mudstones of Namunagarh Grit exhibiting deformational structures that closely resemble those reported from convergent margin accretionary complex (Bandopadhyay, 2012). Both the prism and fan sediments were juxtaposed during reactivation of the Jarawa Thrust and telescoped into a high rising, N-S trending fold-thrust belt.

To the east of the Jarawa Thrust, overlying the volcanic series of the ophiolites, five tectono-stratigraphic units are recognized (Karunakaran, 1968) (Fig. 2), consisting of (i) Upper Cretaceous (Campanian) radiolarian chert and siliceous mudstone interbedded with hemipelagic limestone (Bandopadhyay and Ghosh, 1998; Jafri et al., 1993; Ling et al., 1996); (ii) middle Palaeocene–middle Eocene (~60–40 Ma) shallow-marine volcaniclastic conglomerates, sandstones, and biohermal and biostromal limestones of the Namunagarh Grit (Bandopadhyay and Carter, 2017a; Bandopadhyay et al., 2009; Bandopadhyay, 2005); (iii) middle Eocene radiolarian chert and siliceous mudstone (Ling et al., 1996;

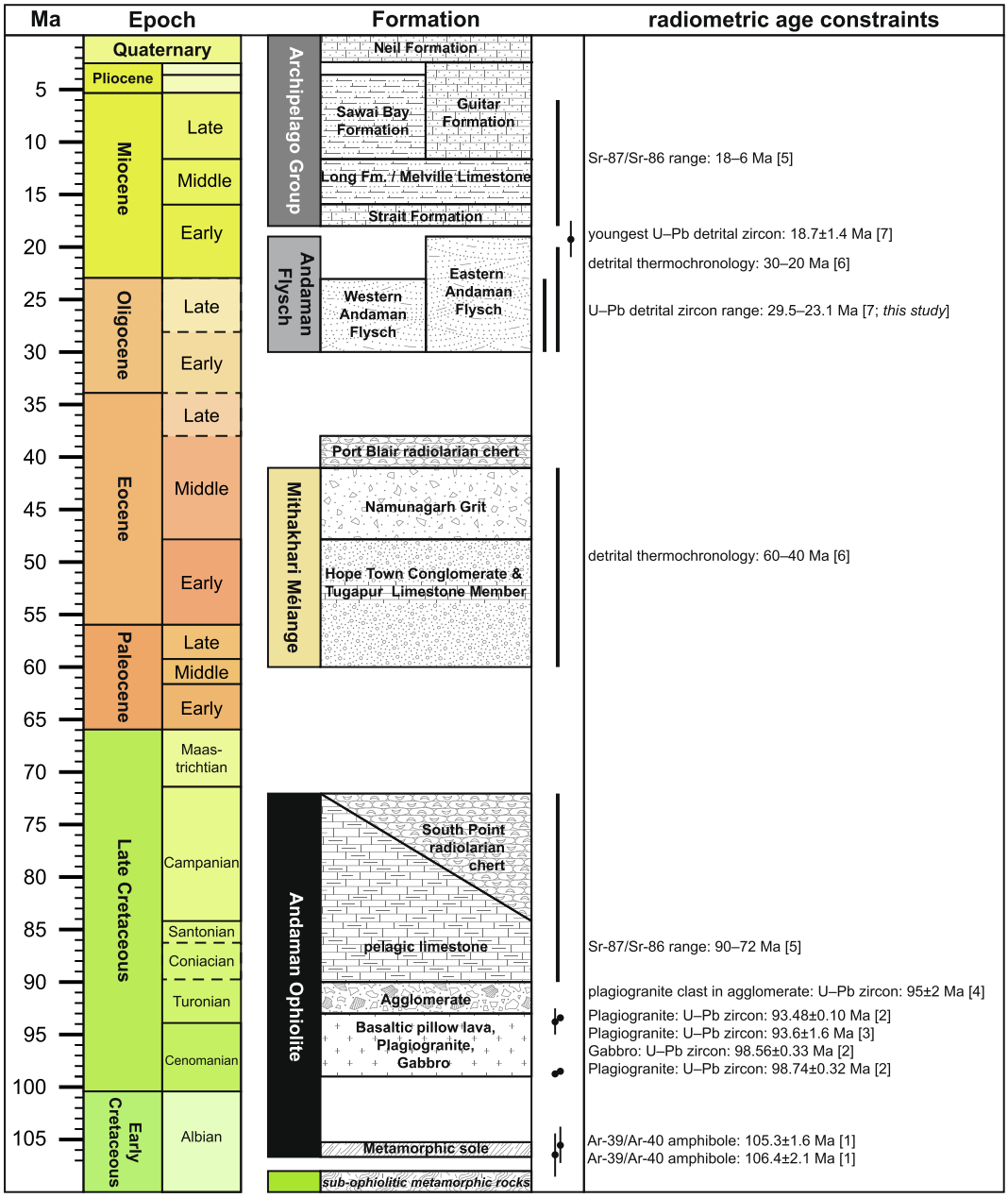

Fig. 2. Chronostratigraphic diagram of the Andaman-Nicobar Islands, showing lithology and biostratigraphic age range of formations within the Andaman Ophiolite, Mithakhari Mélange, Port Blair radiolarian chert, Andaman Flysch, and Archipelago Group. Additional radiometric age constraints from [1] Plunder et al. (2020); [2] Bandyopadhyay et al. (2021); [3] Sarma et al. (2010); [4] Pedersen et al. (2010); [5] Awasthi and Ray (2020); [6] Allen et al. (2008); and [7] Limonta et al. (2017).

Ling and Srinivasan, 1993); (iv) deepwater turbiditic siliciclastic sandstones of the Andaman Flysch of early Oligocene–early Miocene age (Allen et al., 2008; Bandopadhyay and Carter, 2017b; Bandopadhyay and Ghosh, 2015; Limonta et al., 2017; Mukhopadhyay et al., 2003); and finally (v) the Mio-Pliocene archipelago Group with deeper-water shelf deposits consisting of mudstones with several thin intervals of reworked felsic tuffs, shallowing upwards into mixed siliciclastic-carbonate sediments including bioclastic limestones that formed in intertidal setting (Awasthi, 2017; Bandopadhyay and Carter, 2017c). This stratigraphy thus reveals periods of rapid uplift and subsidence accompanied by recurrence of carbonate sedimentation during Palaeocene-Eocene and Mio-Pliocene with a hiatus in Oligocene.

The highest stratigraphic unit of the Andaman Ophiolite is formed by Upper Cretaceous (Campanian) radiolarian chert and siliceous mudstone that are in close association with basaltic pillow lavas on South Andaman Island (Jafri et al., 1993; Ling et al., 1996) (Fig. 3A, B). Geochemistry of these bedded chert suggest deposition near a continental margin (Jafri et al., 1993). Hemipelagic carbonates in close association with these cherts yielded a $^{87}Sr/^{86}Sr$ ratio that suggested a depositional age range of 90–72 Ma (Awasthi and Ray, 2020).

The radiolarian cherts are overlain by the Namunagarh Grit which consists of debritic conglomerates and turbiditic sandstones deposited in discrete and fault-controlled basins fed by small fans in a shallow-water setting (Bandopadhyay and Carter, 2017a; Bandopadhyay, 2005; Chakraborty, 1999). This formation is in many places along the east coast of the islands overthrust by sub-ophiolitic melange, and the two are often collectively referred to as the Mithakhari Mélange (Bandopadhyay and Carter, 2017a).

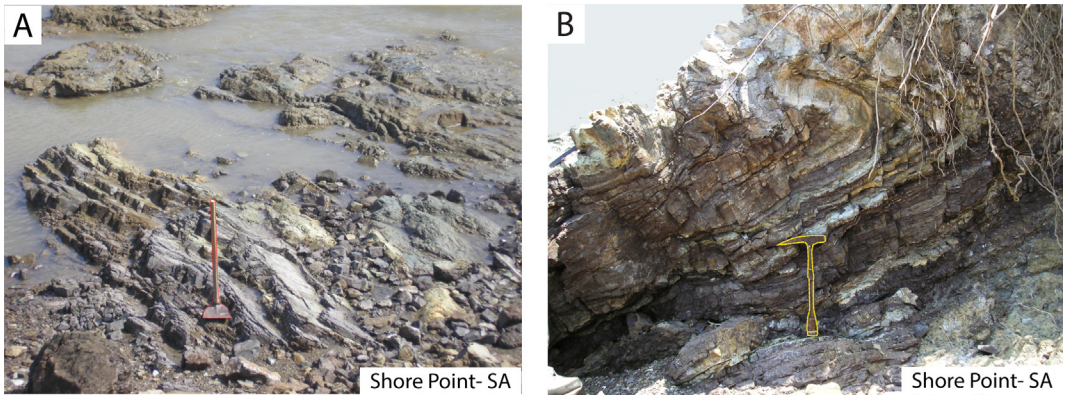

Fig. 3. Radiolarian chert and siliceous mudstone forming up to 2 m thick sequences (A); Slumped bedded chert from the Shore Point, South Andaman, containing Late Cretaceous (Campanian) radiolaria (B).

The matrix-supported and massive, occasionally graded, bedded conglomerates are both oligomictic and polymictic. The former consists of lime or quartz pebble conglomerates with planner clast fabric, implying emplacement by cohesive debris flows. The ophiolite-derived and reworked sedimentary components in polymictic conglomerates comprise both rounded and angular clasts. The rounded pebbles indicate reworking in high-energy environments possibly in fluvial channels, before being deposited in a shallow marine setting (Bandopadhyay and Ghosh, 1998). Turbidites, an important provenance tracer, and the major lithofacies of the Namunagarh Grit, comprise pebbly (gritty) sandstones, coarse to medium-grained and finer-grained calcareous and tuffaceous sandstones/siltstones including tuffs. Field studies in South, Middle and North Andaman Islands have revealed that the Namunagarh Grit turbidites (Fig. 1C, Table 1), in contrast to monotonous sandstone-mudstone successions of Andaman Flysch turbidites, show a varied combination of conglomerate-sandstone-mudstone in different islands, correlatable to facies models established for turbidites of submarine fan complexes (Shanmugam and Moiola, 1988) and of significant provenance and paleogeographic implications. In South Andaman these are 1), thick and massive conglomerate filling channel cut into the bedded sandstone and the succession is devoid of mudstone interbeds (Fig. 4A), and 2) non-channelized, medium-thick and deformed beds of sandstones interbedded with equally thick beds of mudstone (Fig. 4B). Thin-bedded turbiditic sandstones and mudstones dominate in Middle Andaman (Fig. 4C), except Karmatang beach that preserves small scale cyclicity in turbiditic successions (Fig. 4D). Interbedded sandstone-mudstone couplets on the Kalipur and Smith island beaches in North Andaman represent different kinds of turbidites (Bandopadhyay and Carter, 2017a) (Fig. 4E, F). Normal grain-size grading, low dipping beds, fluid-escape structures (disk, vertical pipes), rip-up mudstone clasts, unreworked body fossils, large benthic foraminifera, and ichnofossils in sandstones beds, collectively indicate deposition by turbidity currents in a shallow-water basin (Bandopadhyay, 2012). A deltaic to shallow-marine depositional environment has also been proposed (Chakraborty, 1999). Conglomerate clast lithologies indicate plutonic, volcanic, metamorphic, and sedimentary sources. The variations in clast population imply variable supply from the source and in turn reactivation of the source terrane tectonism. *Nummulites*-rich foraminiferal limestone (patch reef) reveal an early–middle Eocene age (late Ypresian to early Lutetian; Bandopadhyay and Carter, 2017a; Bandopadhyay, 2012). This age is consistent with biostratigraphic constraints showing upper Paleocene to middle Eocene age (Chatterjee, 1964) and maximum depositional ages in the ~60–40 Ma time interval suggested by detrital zircon U–Pb ages and apatite fission track dating (Allen et al., 2008; Bandopadhyay and Carter, 2017a). Paleocurrent patterns are in modern orientations highly variable (Chakraborty, 1999; Karunakaran, 1968), which may reflect deposition in small, discrete fault controlled basins (Allen et al., 2008), although the role of intense deformation in dispersing an originally more coherent paleocurrent pattern is difficult to assess.

In close association with the Andaman Ophiolite and the Namunagarh Grit are local exposures of middle Eocene radiolarian chert and siliceous mudstone on South Andaman (Ling et al., 1996; Ling and Srinivasan, 1993). These cherts signal rapid subsidence and sediment starvation during the middle Eocene.

The East Andaman Flysch (EAF), i.e. to the east of the Jarawa Thrust is not widely exposed. Only on South Andaman, in key sections in Mazar, South Point, and Corbyn's Cove (Fig. 1C, Table 1), there are unequivocal East Andaman Flysch occurrences. These are intensely faulted, folded, and in places either vertical or overturned (Fig. 5A, B, C). The East Andaman Flysch consists of tabular-bedded turbiditic sandstones with partial or complete Bouma sequences interbedded with mudstones of basinal origin, which reach a thickness of ~250 m (Bandopadhyay and Carter, 2017b; Bandopadhyay, 2012). To the west of the Jarawa Thrust, the West Andaman Flysch (WAF) sandstones are the only lithology intermittently exposed (Fig. 1C, Table 1) all along the west coast from northern tip of North Andaman to southern tip of Great Nicobar Island. The rocks are folded into coherent, N-S trending antiforms and synforms with a ~500 m wavelength that appear to have undergone much less complex deformation than in the east (Bandopadhyay, 2012) (Fig. 5D, E, F). The sedimentary facies of the Andaman Flysch on both sides of the Jarawa Thrust are similar and the units have therefore been mapped as a single formation. However, the flysch west of the Jarawa Thrust (West Andaman Flysch) was likely deposited on the Indian Plate and later incorporated into the accretionary prism, whilst the East Andaman Flysch overlying the Namunagarh Grit Formation was deposited in a forearc, and may thus have a very different provenance, or age. We therefore treat the two units separately and use the outcrop of the Jarawa Thrust as boundary between the West Andaman Flysch and the East Andaman Flysch. There are no reliable biostratigraphic dates for the East Andaman Flysch or West Andaman Flysch. Deposition of the East Andaman Flysch between 30 and 20 Ma was inferred for the Corbyn's Cove section based on $^{40}Ar/^{39}Ar$ detrital mica, and detrital apatite and zircon fission track dating (Allen et al., 2008). Limonta et al. (2017) reported detrital zircon U–Pb ages as young as 19 Ma from one East Andaman Flysch section at Dundus Point, nearby Corbyn's Cove (Table 2).

Table 1
Key geographic locations referred in the text as well as location of samples collected for Laboratory study from the Andaman & Great Nicobar Islands.

Point[†]	Location	Lat - Long	Sample Number [Geochronology sample]	Lithology	Laboratory studies done on sample
East Andaman Flysch					
1	Mazar, SA	11°39′04″N; 92°45′20″E	Anf/maz/1	Quartzose (Qt) greywacke with volcanic detritus	Geochemistry + XRD
2	Chidiyatapu, SA	11°30′24″N; 92°40′30″E	Anf/chi/1	Qtz arenite	Geochemistry
3	Goltikdi, Baratan Is.	12°09′02″N; 92°50′48″E	Anf/gol/1 [ANF(E)GOL17]	Mudstone/shale	Geochemistry + U-Pb dating + XRD
4	Corbyn's Cove, SA	11°39′00″N; 92°45′00″E	Anf/f/s/1	Mudstone/shale	Geochemistry + XRD
			Anf/cor/1	Qt graywacke	Geochemistry + XRD
			Anf/cor/2	Qt graywacke	Geochemistry + XRD
			Anf/cor/mud/1	Mudstone/Shale	Geochemistry + XRD
			Anf/cor/3	Qt graywacke	Geochemistry
5	Brindaban School, SA	11°43′11″N; 92°40′11″E	Anf/bri/1	Qt graywacke	Geochemistry
6	Dundus Point, SA	11°40′15″N; 92°42′00″E	Anf/dan/1 [ANF(E)DAN17]	Qt graywacke	Geochemistry + U-Pb dating
7	North-bay, SA	11°42′17″N; 92°45′06″E	Anf/n.bay/1	Qt graywacke	Geochemistry
8	Austin Creek, MA	12°53′31″N; 92°50′32″E	Anf/aus/1	Qt graywacke without volcanic detritus	Geochemistry
West Andaman Flysch					
9	Collinpur, SA	11°41′39″N; 92°35′50″E	Anf/col/1 [ANF(W)COL17]	Calcareous graywacke	Geochemistry + U-Pb dating
10	Bandhan Nala, NA	13°25′46″N; 92°53′02″E	Anf/ban/1 [ANF(W)BAN17]	Calcareous Quartzwacke	Geochemistry + U-Pb dating
11	Talbagan, MA	13°14′23″N; 92°51′07″E	Anf/tal/1	Qt graywacke	Geochemistry
12	Bara Khari, Rutland Is.	11°25′25″N; 92°37′42″E	Anf/rut/1 [ANF(W)RUT17]	Calcareous Quartzwacke	Geochemistry + U-Pb dating + XRD
13	Wandoor, SA	11°35′45″N; 92°36′ 28″E	Anf/wan/1	Calcareous Quartzwacke	Geochemistry + XRD
14	Kaushalyanagar, MA	12°31′37″N; 92°49′53″E	Anf/w/kau/17 [ANF(W)KAU17]	Quartzose graywacke	U-Pb dating
Namunagarh Grit					
15	Kalighat Diversion, NA	13°10′46″N; 92°55′41″E	Nam/kd/m/3	Quartz-poor sandstone with significant amount of volcanic grains	Geochemistry + XRD
			Nam/kd/m/3/1	Quartzofeldspathic with andesite grains	Geochemistry + XRD
16	Hopetown, SA	11°41′41″N; 92°43′50″E	San/ht/1	Tuffaceous sand stone and tuffs	Geochemistry
			San/ht/2	Tuffaceous sand stone and tuffs	Geochemistry
17	Sippy Ghat, SA	11°36′17″N; 92°39′54″E	San/s.ghat/1	Tuffaceous sand stone and tuffs	Geochemistry
18	Namunagarh, SA	11°41′34″N; 92°41′11″E	Sa/nam/1	Bedded Tuff	Geochemistry + XRD
2	Chidiyatapu, SA	11°30′24″N; 92°40′30″E	Sa/nam/chi/2	Mudstone/shale	Geochemistry + XRD
19	Karmatang Beach, MA	12°50′44″N; 92°56′08″E	Man/kar/b/2 [ANM(N)KAR17]	Quartzofeldspathic with andesite grains	Geochemistry + U-Pb dating
		12°50′44″N; 92°56′09″E	Man/kar/b/1	Quartzofeldspathic with andesite grains	Geochemistry + XRD
		12°51′13″N; 92°56′05″E	Man/kar/b/mud/1	Mudstone/shale	Geochemistry + XRD
20	Smith Is., NA	13°18′37″N; 93°04′15″E	Nam/smi/1/mud	Mudstone/shale	Geochemistry + XRD
		13°18′38″N; 93°04′15″E	Nam/smi/sst/2	Quartzofeldspathic with andesite grains	Geochemistry
		13°18′38″N; 93°04′51″E	Nam/smi/sst/1	Quartzofeldspathic with andesite grains.	Geochemistry + XRD
21	Kalipur, NA	13°13′17″N; 93°02′35″E	Nam/kal/1	Quartzofeldspathic with andesite grains	Geochemistry + XRD
22	Panchawati, MA	12°34′45″N; 92°57′41″E	No sample collected; location referred in the text		
23	Ramnagar Beach, NA	13°04′30″N; 93°01′34″E			
24	Tugapur, MA	12°51′46″N; 92°48′04″E			
West Andaman Flysch (Great Nicobar Is.)					
25*	Jogindarnagar	06°58′55″N; 93°51′11″E	Anf/nic/l-2 [ANF(W)NIC17]	Quartzose graywacke	Geochemistry + U-Pb dating
26*		07°00′45″N; 93°55′07″E	Anf/nic/l-3	Quartzose graywacke	Geochemistry

[†] Refers to the location point marked in Fig. 1C; *Not shown in Fig. 1C.

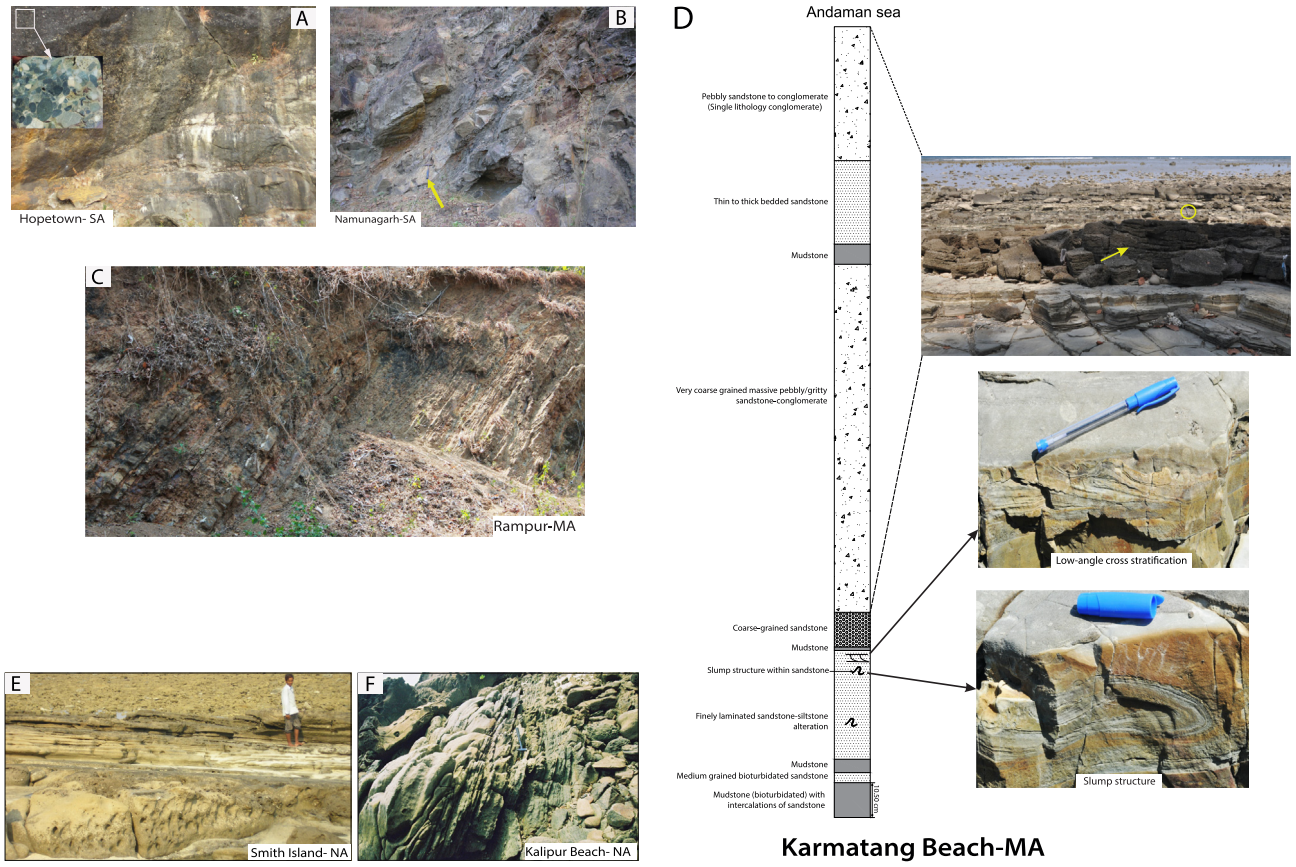

Fig. 4. Turbidites of the Namunagarh Grit recognized in South, Middle, and North Andaman Islands of varied paleogeographic setting. A) A channel cuts the bedded sandstones and is filled with massive petromict orthoconglomerates; polished slab of petromict conglomerate (length 5 cm) with well-rounded to angular grains (inset). They correspond to proximal inner fan deposit of a fan delta, SA. B) Turbidites from Namunagarh quarry section, South Andaman; non-channelized parallel-stratified beds of sandstones, gently deformed and interbedded with medium-thick beds of mudstone that was not observed in A. The turbidites most likely represent the deposit of the mid-fan complex. C) Thin bedded sandstone-mudstone of Namunagarh Grit turbidites, Rampur, Middle Andaman. They correspond to distal basin plain succession of the lower fan complex. D) Low (<15°) easterly (seaward) dipping turbidites of Namunagarh Grit exposed on the Karmatang beach, Middle Andaman (top photograph); coarsening and thickening upward motif is expressed in the measured stratigraphic column; middle photograph showing very low angle cross-lamination (=Bouma T_C interval); lower photograph showing sandstone bed with slump structure (=Bouma T_B interval). E & F) Namunagarh Grit turbidites from Smith Island and Kalipur, respectively, North Andaman.

The Archipelago group was recently dated with $^{87}Sr/^{86}Sr$ on Havelock Island to the east of South and Middle Andaman, at 18–6 Ma (Awasthi and Ray, 2020). This group unconformably overlies both the WAF and the EAF, revealing that the juxtaposition of the latter two along the Jarawa Thrust predates the middle-late Miocene. The age of the Archipelago group overlying the WAF, however, has not been directly established and may be younger than on Havelock Island. In places, thrusts emplace the Namunagarh Grit Formation on the Archipelago Group (Bandopadhyay and Carter, 2017c) showing that there was upper plate shortening of the forearc ridge since the late Miocene, and perhaps continuously or intermittently since the Eocene.

Given the current paleogeographic reconstructions for the Cenozoic, there are four main source regions from which the sediments of the Andaman and Nicobar Islands may have been derived. If they were accreted from the Nicobar Fan on the downgoing Indian Plate, they may give a Himalayan-Tibetan and Indian provenance. If deposited in the overriding plate, they may derive from the West Burma Block and overlying arcs and surrounding ophiolites, from the Sundaland continental block and Mesozoic arc assemblage intruded therein, or from Sumatra, including the Lower Cretaceous Woyla Arc (Fig. 1A). Alternatively, they may have been derived from the Alcock and Sewell Rises that may comprise hyper-extended Sundaland continental crust (Morley and Searle, 2017; Morley and Alvey, 2015).

Previous sediment provenance studies identified that the Namunagarh Grit was derived from an active or extinct volcanic arc (Allen et al., 2008; Awasthi, 2017; Bandopadhyay and Carter, 2017a; Bandopadhyay, 2005). Allen et al. (2008) and Awasthi and Ray (2020), in addition, also reported a secondary Precambrian-Palaeozoic continental source and suggested that these may source from the Shan-Thai block in eastern Myanmar (Allen et al., 2008) or the Himalaya (Awasthi and Ray, 2020). The Woyla Arc of Sumatra has hitherto not been discussed as possible sediment source. Sediments of the Andaman Flysch have been suggested to come either from the Irrawaddy River of Myanmar (Bandopadhyay and Ghosh, 2015; Karunakaran, 1968; Pal et al., 2003; Ray, 1982) or from western Myanmar (Chakraborty and Pal, 2001). Alternatively, at least part of the Andaman Flysch has been suggested to represent accreted Bengal Fan material shed from the Himalaya onto the ocean floor east of India (Curray et al., 1979; Curray, 2005). Curray and Allen (2008) and Allen et al. (2008) proposed a recycled orogenic source for EAF samples and considered a contribution from the nascent Himalaya appears very minor. Awasthi and Ray (2020), however, lumping WAF and EAF samples together, considered a Himalayan source likely. There appears to be a consensus that the EAF from Corbyn's Cove was sourced from continental crustal plutonic-metamorphic rocks, perhaps of the Shan-Thai continental blocks or Mogok metamorphic belt NE of the Andaman Islands (Bandopadhyay and Ghosh, 2015; Limonta et al., 2017). In

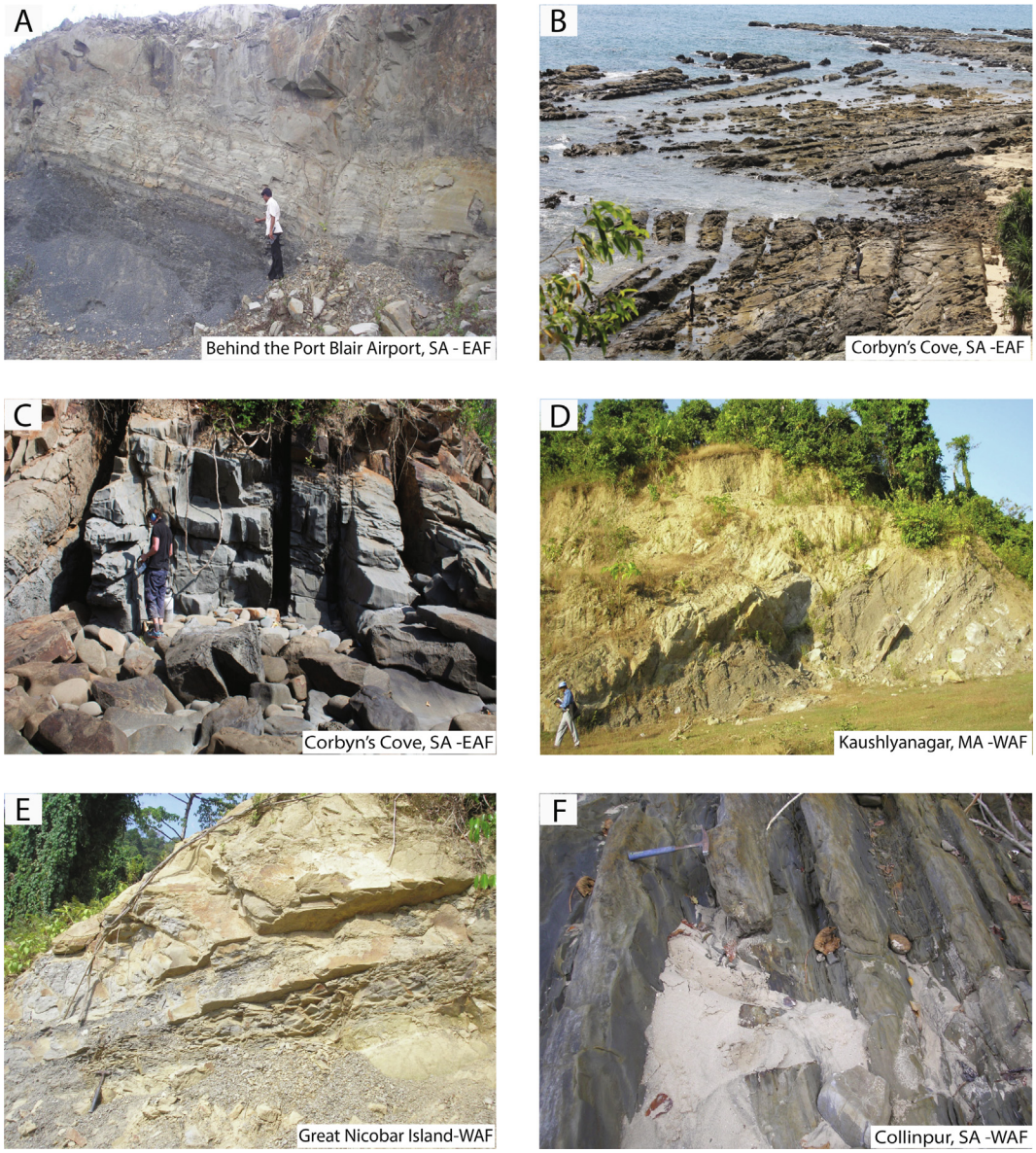

Fig. 5. Deepwater turbidites of Andaman Flysch. A) East Andaman Flysch turbidites exposed due to excavation on a hilly terrain behind the airport, Port Blair. Note the completely overturned sandstone bed > 3 m thick showing massive upper and laminated lower part. B) Aerial view of faulted and fractured East Andaman Flysch exposed during low tide on the wavecut platform, Corbyn's Cove, South Andaman. C) Fresh, and vertical beds of East Andaman Flysch sandstone on sea cliff, Corbyn's Cove, South Andaman; mudstone beds are hardly noticed. D) West Andaman Flysch at Kaushalyanagar, Middle Andaman showing interbedded sandstones and mudstones, sandstone beds are nearly undeformed and thicken up-section. E) West Andaman Flysch turbidites of Great Nicobar Island showing very thick and internally structureless beds of sandstone alternating with much thinner beds of fissile mudstone. F) A typical normal succession of West Andaman Flysch turbidites on the Collinpur beach, west of South Andaman showing sandstone-mudstone alternations; both beds are almost equally thick.

summary, the provenance of the Andaman Flysch is not well agreed upon, perhaps as a result of lumping two formations of different provenance.

3. Sampling and methods

3.1. Sampling

We collected medium to fine-grained sandstones from exposures of the Namunagarh Grit Formation and the East and West Andaman Flysch, distributed along the 700 km long belt from North Andaman to Great Nicobar (Table 1). Conglomerate clast compositions were studied in the field. Samples were assigned to formations, but the discontinuous and limited exposure leaves relative stratigraphic positions or our samples within formations unconstrained.

Sandstone samples were collected for bulk sediment petrography in thin section. Range and average concentrations of major oxides, trace elements and Rare Earth elements (REE) from bulk samples were determined on a selection of 33 samples that include nine sandstone and three mudstone samples from East Andaman Flysch, seven sandstone samples from West Andaman Flysch (five from the Andaman and two from the Great Nicobar Island), and eleven sandstone and three mudstone samples from Namunagarh Grit. XRD analysis was carried out on 17 samples (6 from East Andaman Flysch, 2 from West Andaman Flysch and 9 from Namunagarh Grit). Zircon U-Pb age dating was performed on five samples from the West Andaman Flysch (four from the Andaman and one from the Great Nicobar Island), one from the Namunagarh Grit

Table 2
Synthesis of sedimentary rocks analyzed for U-Pb dating.

Sample Name	Source	Latitude- Longitude	Location	Zircon Maximum depositional Age (n ≥ 3)	Youngest zircon age
West Andaman Flysch					
ANF(W)NIC17	This Study	06°58′55″N; 93°51′11″E	Jogindarnagar, Great Nicobar Island	43.5 ± 3.6 Ma (2 s, n = 3, MSWD = 1.4)	23.1 ± 1.4 Ma (2 s)
ANF(W) RUT17	This Study	11°25′25″N; 92°37′42″E	Bara Khari, Rutland Island	29.5 ± 1.9 Ma (2 s, n = 3, MSWD = 3)	23.1 ± 1.2 Ma (2 s)
ANF(W) KAU17	This Study	12°31′37″N; 92°49′53″E	Kaushalyanagar, MA	44.8 ± 1.5 Ma (2 s, n = 7, MSWD = 1.9)	41.9 ± 1.5 Ma (2 s)
ANF(W) BAN17	This Study	13°25′46″N; 92°53′02″E	Bandhan Nala, NA	51.5 ± 3.8 Ma (2 s, n = 3, MSWD = 4.4)	34.2 ± 1.1 Ma (2 s)
ANF(W) COL17	This Study	11°41′39″N; 92°35′50″E	Collinpur, SA	50.6 ± 1.5 Ma (2 s, n = 4, MSWD = 0.7)	28.8 ± 1.1 Ma (2 s)
AND9	Limonta et al. (2017)	06°58′55″N; 93°51′11″E	Great Nicobar Island	473.2 ± 13.7 Ma (2 s, n = 3, MSWD = 0.3)	44.0 ± 1.9 Ma (2 s)
AND5	Limonta et al. (2017)	11°25′24″N; 92°37′23″E	Rutland Island	51.6 ± 3.1 Ma (2 s, n = 4, MSWD = 3.6)	24.1 ± 1.6 Ma (2 s)
AND17	Limonta et al. (2017)	N/A	Luckno, MA	218.4 ± 9.8 Ma (2 s, n = 4, MSWD = 2.7)	54.5 ± 3.8 Ma (2 s)
East Andaman Flysch					
ANF(E)GOL17	This Study	12°09′02″N; 92°50′48″E	Goltikdi, Baratan Island	42.7 ± 1.1 Ma (2 s, n = 22, MSWD = 1.1)	41.6 ± 2.1 Ma (2 s)
ANF(E)DAN17	This Study	11°40′15″N; 92°42′00″E	Dundus Point, SA	72.3 ± 4.8 Ma (2 s, n = 3, MSWD = 2.6)	21.1 ± 0.8 Ma (2 s)
AND3	Limonta et al. (2017)	11°40′14″N; 92°42′00″E	Dundus Point, SA	19.2 ± 0.8 Ma (2 s, n = 3, MSWD = 1)	18.7 ± 1.4 Ma (2 s)
AND6	Limonta et al. (2017)	12°53′31″N; 92°50′32″E	Austin Creek, MA	46.6 ± 3.9 Ma (2 s, n = 3, MSWD = 3.4)	45.6 ± 1.8 Ma (2 s)
CC	Limonta et al. (2017)	11°38′27″N; 92°45′19″E	Corbyn's Cove,SA	40.5 ± 2.8 Ma (2 s, n = 3, MSWD = 2.4)	39.5 ± 1.7 Ma (2 s)
Namunagarh Grit					
ANM(N) KAR17	This Study	12°50′44″N; 92°56′08″E	Karmatang Beach, MA	218.7 ± 6.4 Ma (2 s, n = 10, MSWD = 1.8)	212.2 ± 8.2 Ma (2 s)
Hopetown	Limonta et al. (2017)	11°41′41″N; 92°43′50″E	Hopetown Conglomerate, SA	59.5 ± 1.6 Ma (2 s, n = 20, MSWD = 1.3)	55.9 ± 2.0 Ma (2 s)
Namunagargh	Limonta et al. (2017)	11°41′34″N; 92°41′11″E	Namunagargh Quarry, SA	43.4 ± 1.7 Ma (2 s, n = 6, MSWD = 1.4)	41.2 ± 2.9 Ma (2 s)

Three NG samples from the Kalipur coast (2) and Mugleton (1) from Bandopadhyay and Carter (2017a) are not displayed because of low zircon number (n < 80).

Formation, two from the East Andaman Flysch. Locations and key characteristics of all samples are given in Table 1.

3.2. Analytical procedures

Whole-rock major, trace and REEs were analyzed by X-ray fluorescence spectrometry (XRF) and by inductively coupled plasma-mass spectrometry (ICP-MS) at the Department of Earth Sciences, University of Utrecht. Each sample was powdered (<-200 mesh) using a cup and Ball-Mill pulveriser of the Hertzog (HP-MA) milling machine. Loss of ignition (LOI) was determined at 900 °C for 9 min using the method described by Lechler and Desilets (1987). Fused glass discs were prepared for major element analysis by XRF following methods described by Ahmedali (1989) and Longerich (1995). The analytical precision is better than 5% for major oxides. Trace elements data including REE were obtained with slandered ICP-MS procedures following (Jenner et al., 1990). Accuracy and precision were estimated and monitored from the controlled samples and duplicates. The precision of the replicate analysis is better than 5% for all analysed trace elements. The entire geochemical dataset along with the compilation from the previous literatures (Awasthi 2017; Bandopadhyay & Ghosh, 1998; Bandopadhyay & Ghosh, 2015; Bandopadhyay and Carter, 2017b) is given in the Supplementary Table 1.

To study the composition and characteristics of clay minerals, we used the clay (<4 μm) fraction of sandstones and interbedded mudstones (shales). The clay fraction of each sample was divided in two and treated with either a 1 M KCl solution or a 0.1 M $MgCl_2$ solution. The samples were then mounted on glass slides and allowed to dry at room temperature. After measuring the air-dried slides, we heated the K-saturated mounts to 550 °C and solvated the Mg-saturated mounts with ethylene glycol at 60 °C and remeasured the slides. The samples were run on a Bruker D2 Advance with a θ/θ goniometer using Co-*K*α radiation (30 kV/10 mA) at the Debye Institute for Nanomaterials Science, Utrecht University. We used a primary Soller slit of 2.5° and a 1 mm divergence slit. The illite crystallinity (IC) in different illite-bearing samples was measured using the Weber Index (Weber, 1972), and the Kubler Index (Kübler, 1968).

U-Pb geochronology of zircons was conducted by laser ablation inductively coupled plasma mass spectrometry (LA–ICP-MS) at the University of Washington. Analytical procedure is detailed in Licht et al. (2020). Briefly, zircon crystals were extracted by traditional methods of heavy mineral separation, including concentration with a Holman-Wilfley gravity table, density separation with methylene iodide, and magnetic separation. U-Pb dates were generated using an iCAP-RQ Quadrupole ICP-MS coupled to an Analyte G2 excimer laser, with a spot diameter of 25 μm. Data reduction was conducted with *Iolite*, using their *U_Pb_Geochron4* data reduction scheme to calculate U-Pb dates uncorrected for common lead (Paton et al., 2010). Dating uncertainties for all samples were calculated using an in-house *Matlab* script that follows the most recent recommendations for U-Pb age reduction (Horstwood et al., 2016). The ten zircon validation reference materials used during these sessions yielded offset around TIMS ages < 1% in most cases, <2% otherwise.

We calculated the maximum depositional age for each sample (as well as the samples from Limonta et al., 2017; Table 2) as the

weighted average of the youngest zircon dates when the youngest three or more dates overlap (Dickinson and Gehrels, 2009), using *Tuffzirc* (Ludwig, 2003). The final age uncertainty around maximum depositional ages is the quadratic sum of the uncertainty of *Tuffzirc* age calculation or youngest zircon date and of the systematic uncertainty (~2.67% for the $^{238}U/^{206}Pb$ ratios). Age distributions are given in the form of kernel density estimate (KDE) diagrams and age histograms obtained with *Matlab*. Ages were screened for concordance using a discordance filter at > 20% discordance (<80% concordance) and > 5% reverse discordance (>105% concordance); we used the $^{206}Pb/^{238}U$ vs $^{207}Pb/^{235}U$ ratio to calculate discordance for dates < 1300 Ma, and the $^{206}Pb/^{238}U$ vs $^{207}Pb/^{206}Pb$ ratio for older dates. In total, our new dataset includes 2451 concordant zircons ages; detailed data are provided in Supplementary Table 2.

4. Results

4.1. Sample petrography and clay mineralogy

Namunagarh Grit sandstones consist of tuffs (neovolcanic), tuffaceous sandstones (mixed paleovolcanic and plutonic-metamorphic), and arkoses (Fig. 6). Tuffs rich in juvenile grains are exclusively present in the Namunagarh Grit of South Andaman Island, whereas Namunagarh Grit sandstones from Middle and North Andaman are tuffaceous. Juvenile grains in tuffs include vitric volcanic lithic grains (glass shards), whole or broken plagioclase phenocrysts showing magmatic zoning, and angular grains of andesite with microlitic, felsitic, and lathwork textures; a few comprise felsitic and basaltic grains (Fig. 6A-H). Ferromagnesian minerals, though rare, include euhedral long prismatic crystal of oxyhornblende and short prismatic pyroxenes likely of andesitic parentage (Fig. 6H). Framework grains are embedded in a smectite-chlorite matrix. These framework matrix assemblages are characteristic of a synvolcanic/neovolcanic source (Fisher and Schmincke, 1984). Volcanic spherules in tuffs bear evidence of high temperature devitrification.

The tuffaceous sandstones of the Namunagarh Grit (Fig. 6I-P) contain significant amounts of sand grains derived from plutonic-metamorphic (mono and polycrystalline quartz, feldspar, and muscovite) and sedimentary sources (sand-sized lithic grains of fine mudstone, siltstone, radiolarian chert, and micritic limestone, as well as sand grains of feldspar and rounded quartz) mixed with andesite lithic grains of a paleovolcanic source. Mica grains, seldom recorded in andesitic volcanic rocks, are conspicuous in some samples and indicate contribution from a metamorphic source (Fig. 6C, D). Strongly sutured subgrain boundaries in polycrystalline quartz grains (Fig. 6O) convey derivation from high-grade metamorphic rocks. An average plagioclase-total feldspar ratio of 0.91 indicates that plagioclase is more abundant than K-feldspar in the tuffs and tuffaceous sandstones, suggesting an intermediate volcanic source (Critelli and Le Pera, 1994).

XRD clay mineralogy reveals that smectite, in this case a fully crystalline form of palagonite (Spears, 1982), and 14 Å chlorite are common matrix minerals in Namunagarh Grit sandstones (Fig. 7 and Table 3). The sandstones show minor diagenetic changes possibly due to early calcite cementation and/or short distance transport. Values of IC > 1 in six Namunagarh Grit samples indicate shallow diagenesis (Verdel et al., 2012).

In summary, petrography highlights the pyroclastic and mixed pyroclastic-epiclastic compositions of the Namunagarh Grit sandstones, likely derived from an andesitic arc, and a post-eruptive sediment source that also includes exhumed and uplifted plutonic-metamorphic rocks of deeper crustal levels.

East Andaman Flysch sandstones are dominantly quartz (gray) wackes, and some are lithic arenites. Modal analyses (Table 4) based on published data revealed strong variation in volume% of lithic grains (28% for Corbyn's Cove; Allen et al., 2008), but only 7% for nearby Dundus Point and Brindaban; Limonta et al., 2017) reflecting abrupt shift of source areas. Lithic grains, often deformed, range from micaceous metamorphic grains, diagnostic of continental sources, to a few grains of altered basalts possibly derived from ophiolitic sources. Staurolite, considered a tracer mineral of a Himalayan provenance (Najman et al., 2009) is present only in one sample. Framework grains are moderately to tightly packed in an illite-muscovite matrix (Fig. 8A). Rounded mono- and polycrystalline quartz and chert grains exhibit the characteristics of recycled sedimentary grains (Basu, 1985; Pettijohn et al., 1987) (Fig. 8B). Polycrystalline quartz shows either interlocking subgrain contacts or long sutured contacts with preferred orientation of the subgrains. The former was possibly derived from a plutonic source while the latter may indicate a high-grade metamorphic source (Fig. 8C, D). Non-undulose monocrystalline grains of plutonic origin are more abundant than undulose (undulosity > 5°) grains of low-rank metamorphic sources (Basu, 1985). Quartz grains, with inclusions of zircon and apatite, and perthite grains interpreted as plutonic igneous source (Morton and Hallsworth, 1994; Pittman, 1970) represent a substantial contribution to the bulk composition, as do hydrothermal quartz grains (Shepherd et al., 1985; Tucker, 2009), which appear dusty due to fluid inclusions, forming thin strings throughout the grain. Allen et al. (2008) reported ~5 to 8% altered volcanic fragments.

The East Andaman Flysch sandstones show clear evidence of deep burial diagenesis, showing crude foliation at places defined by parallel orientation of framework grains including muscovite flakes (Fig. 8E). Chlorite/illite/muscovite/sericite form the matrix minerals and locally framework components are embedded in a ferruginous cement. During early shallow diagenesis, feldspar, muscovite, and biotite were altered along and across the cleavage planes and fractures which resulted in formation of illite-muscovite (identified by XRD). Diagenetically altered quartz in most sandstones shows diffuse grain margins fading into the matrix. Later, during mesodiagenesis, increased overburden pressure caused ductile deformation of labile grains and micas, resulting in the formation of pseudomatrix (Dickinson, 1970).

In summary, petrographic data indicate that the East Andaman Flysch matrix-rich quartz (gray)wackes, despite the dominant contribution of detritus from sedimentary and low-grade metasedimentary rocks, contain detritus derived from high-grade metamorphic and volcanic rocks. The sandstones underwent deep burial diagenesis showing that much of the original overburden has been eroded. Sedimentary and metasedimentary lithic grains, though poorly preserved, indicate supra-crustal and crustal sources and sparse volcanic rock sources linked to recycled orogenic provenance likely associated with an active continental margin tectonic setting (Dickinson, 1985).

West Andaman Flysch sandstone compositions vary from mainly lithic arenites to arkoses. Limonta et al. (2017) mentioned lithic, feldspathic, and quartzose to feldspathic-quartzose compositions with lithic fragments making up 8 vol%. Compared to the East Andaman Flysch, the West Andaman Flysch sandstones contain more quartz and fewer (total) feldspar and lithic grains (Table 4). The lithic grains in the West Andaman Flysch are well preserved due to early diagenetic calcite cementation and consist of low to medium rank metasedimentary mudstones and sandstones, that is, metapelite and metapsammite (Garzanti and Vezzoli, 2003). Polycrystalline quartz with flattened subgrains and strongly sutured subgrain contacts bear the clear signal of the presence of high-grade metamorphic rocks in the source region. Muscovite schist, quartz-muscovite-sericite schist, metaquartzite, siltstone

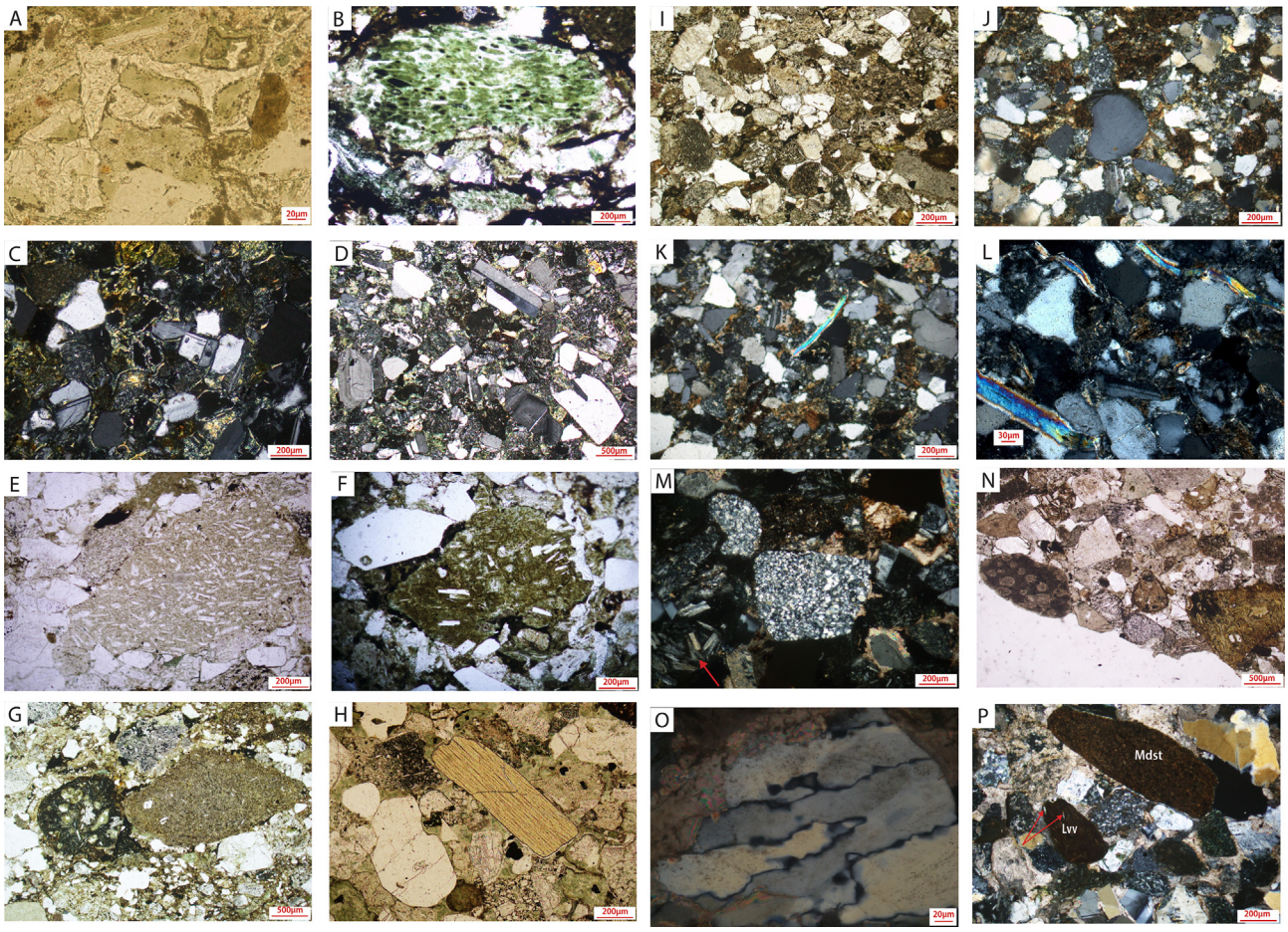

Fig. 6. Photomicrographs of Namunagarh Grit andesitic tuffs and tuffaceous sandstones from different islands of Andaman. (A) Vitric volcanic lithic (Lvv) sandstone composed of large and small nonvesicular glass shards of tricuspate, attenuted, rectangular to irregular shape. (B) Vesicular glass shard showing densely populated and flattened, elliptical vesicles filled with clay minerals with green colour and low-order birefringence; the other components include single crystals and Lvv lithic grains. Both A and B are from Namunagarh, South Andaman suggesting a *syn*-eruptive source and very short transport distance from the source. (C) Crystal-vitric andesitic tuff composed of fresh euhedral to subhedral plagioclase phenocrysts and glass shards showing faint alteration rinds along their grain boundaries; clay minerals with bright birefringence possibly indicate original palagonite recrystallized to smectite. (D) Crystal tuff composed of assorted, whole and broken euhedral-subhedral fresh plagioclase phenocrysts randomly distributed in a chlorite-smectite matrix. Both C and D are from Sippyghat, South Andaman. (E) Poorly sorted and dominantly angular grains in Namunagarh Grit sandstones with a significant amount of synvolcanic detritus (tuffs) that includes outsized and fresh andesite clasts showing a typical lathwork texture defined by random orientation of plagioclase laths. (F) Poorly sorted lithic grains showing a volcanic lithic grain (dark coloured) containing plagioclase laths in felted orientation and adjacent plagioclase phenocrysts (white). (G) Andesite clasts (light coloured) with phenocrysts of plagioclase and basalt (dark coloured); the groundmass consists of relatively finer-grained sand grains, Sippy Ghat, South Andaman. (H) Undeformed, long prismatic and pale brown amphibole and plagioclase phenocrysts in andesitic tuff, Namunagarh, South Andaman. (I) Tuffaceous sandstones of Middle and North Andaman Islands showing relatively better sorting and rounding of the framework grains composed of lithic grains, coarse and fine-grained subrounded to rounded chert, muscovite, plagioclase, and quartz; andesite clasts show randomly oriented plagioclase laths set in a vitric groundmass that are sourced from paleovolcanic, plutonic, metamorphic, and sedimentary rocks. Karmatang beach section, Middle Andaman. (J) Sandstone with a well-rounded and outsized recycled quartz in the middle of otherwise first-cycle grains, Karmatang beach section, Middle Andaman. (K&L) Tuffaceous sandstones showing the distinctive presence of micas, mostly muscovite, Kalipur beach, North Andaman. (M&N) Two coarsely crystalline well-rounded chert grains (M) and brownish radiolarian chert (N) of sedimentary sources; cellular serpentine in N indicates an ultramafic source, Karmatang beach section, Middle Andaman. (O) Part of a large grain of polycrystalline quartz showing long and deeply sutured subgrain contacts with undulose extinction indicative of derivation from a high-grade metamorphic terrane, Smith Island, North Andaman. (P) Tuffaceous sandstone with a well-rounded mudstone clast (dark aphanitic groundmass and no phenocrysts) and a similar looking grain with the same aphanitic dark brown groundmass but presence of feldspar microlites (arrowed) that indicate a reworked (paleovolcanic) vitric volcanic lithic grain. Note also the presence of polycrystalline quartz (right corner) composed of anhedral subgrains showing sharp extinction implying plutonic source, Smith Island beach, North Andaman. Photomicrographs A, B, E, F, I, N are in Plane-polarized light (PPL); C, D, G, H, J, K, L, M, O, P in Cross-polarized light (XPL). (For interpretation of the references to colour in this figure legend, the reader is referred to the web version of this article.)

clasts, deformed fine mudstone, and detrital white micas are common lithic grains (Fig. 8F-J). They are likely sourced from an orogenic source (Dickinson, 1985). Staurolite is conspicuous and present in all samples of the West Andaman Flysch, as a key difference with the heavy mineral assemblage of the East Andaman Flysch (Table 4). In these sandstones, polycrystalline quartz showing two distinctly different sizes of subgrains within a single grain, as well as a high ratio of polycrystalline quartz to total quartz suggests metamorphic source (Basu, 1985). The clay mineralogy of the West and East Andaman Flysch is mostly similar (Table 3). Measured values of illite crystallinity (IC) in the West Andaman Flysch are < 1, ranging between 0.2 and 0.5. Such values are equivalent to the boundary zone between late diagenesis and sub-greenschist metamorphic conditions (Frey, 1987).

Great Nicobar Flysch sandstones closely follow the compositional trend of the West Andaman Flysch (Table 4). Quartz, feldspar, lithic grains, and muscovite, in decreasing order of abundance, make up the composition of the framework. Among three samples collected from east, middle, and west of Great Nicobar, the one from the west is high (12 vol%) in muscovite, signalling enhanced input from a metamorphic terrane. Quantitative petrographic analysis of Nicobar sandstones (Limonta et al., 2017)

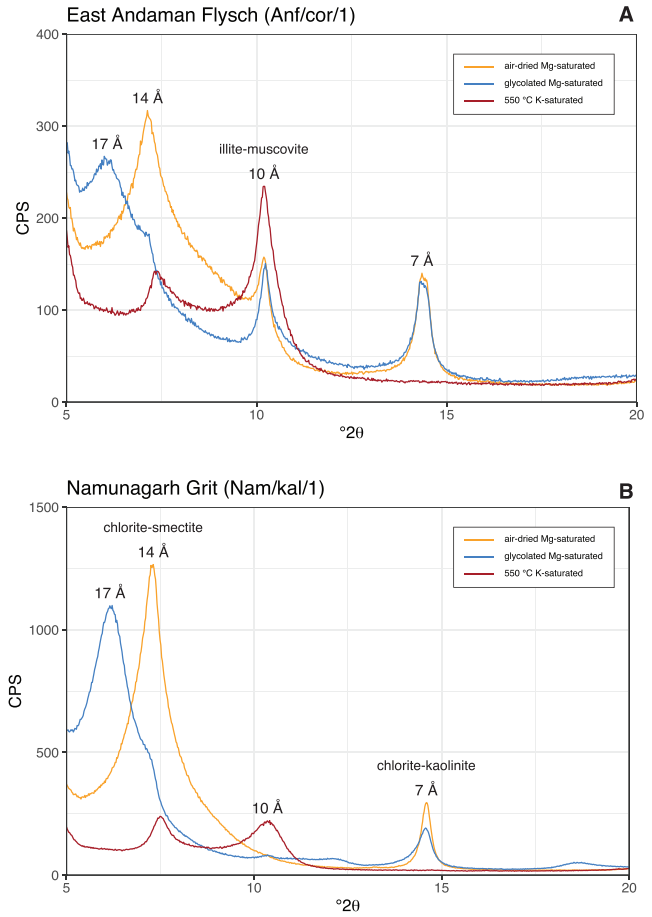

Fig. 7. X-ray diffractograms of oriented mounts of the clay fraction of sandstones. Y-axis in counts per second (CPS). Sharp and prominent 10 Å peaks (illite-muscovite) characterize the clay mineralogy of Flysch sandstones (A) and sharp 14 Å peaks (chlorite and smectite) and 7 Å peaks (2nd chlorite peak and/or kaolinite group) characterize the clay mineralogy of the matrix in NG sandstones (B). Note the virtual absence of mixed layer (ML) clays in all sandstones.

(Table 4) showed that the sandstones are quartz-rich (70.3 vol%) and the detrital modes closely compare to the modal composition of the West Andaman Flysch. Framework pores are filled with illite, muscovite, and sericite (Fig. 8F, G). Sand grains are poorly to moderately sorted and angular. Outsized and well-rounded quartz and chert grains, which resemble recycled grains, and quartz-muscovite schist grains are common components.

In summary, lithic grains of volcanic provenance are recognized in the East, but hardly present in the West Andaman and Nicobar Flysch turbidites. The latter two formations are rich in lithic grains that comprise micaschist, quartz micaschist, quartz-mica-sericite schists with crude schistosity, recycled quartz, metamorphic polycrystalline quartz, and rounded chert. These lithic grains are quite similar to low to medium rank metamorphic lithic grains, such as metamorphic lithic grains with rough cleavage of Tethys Himalaya and quartz-sericite lithic grains with strong cleavage of Lesser Himalaya origin (Garzanti and Vezzoli, 2003).

4.2. Geochemistry

Range and average concentrations of major, trace, and rare earth elements, elemental ratios, and weathering indices for the sandstones and mudstones of the Namunagarh Grit and East and West Andaman Flysch (Supplementary Table 1) were determined and compared with published data, revealing consistency of our analytical data. The major element geochemistry of Namunagarh Grit sandstones indicates that parent rocks were mainly andesites with a few sandstones compared with basaltic andesite and dacite. Also, the K_2O/Na_2O ratios < 1 with an average of 0.29 in sandstones indicate a volcanogenic source (Crook, 1974). Sandstones in total alkali-silica diagram of Le Maitre et al. (2002) (not shown) plot in the andesite (5 samples), dacite (4 samples), and basaltic andesite (2 samples) fields, consistent with the compositional trend of an evolving island arc (Hamilton, 1988). The range and average concentrations of Rb (13.5–56.6, average 24.3 ppm) confirm that the sediment source was dominated by mafic rocks. Also, Th/Sc ratio (0.03–0.46, average 0.13) (Supplementary Table 1) are within the range (0.05–0.22) of sediments derived from mafic sources

Table 3
XRD of clay minerals of sandstone and shale samples of NG, EAF, and WAF, and illite crystallinity values.

Sample number	Group	14 Å peak		10 Å peak	7 Å peak	ML	10 Å peak = 10.25 °2θ		
							CPS		
							FWHM	net height	net area
Anf/maz/1	EAF	C	S	IM	7		0.3	240	90
Anf/gol/1	EAF		S	IM	7		0.4	140	70
Anf/f/s/1	EAF	C		IM	7	ML	0.6	240	240
Anf/cor/1	EAF	C	S	IM	7		0.4	130	60
Anf/cor/2	EAF	C		IM	7		0.4	160	90
Anf/cor/mud/1	EAF	C	S	IM	7		0.2	120	40
Anf/rut/1	WAF	C		IM	7		0.2	150	50
Anf/wan/1	WAF		S	IM	7		0.3	210	100
Nam/kd//m/3	NG		S	IM	7		0.3	60	30
Sa/nam/1	NG	C			7		>1	20	30
Man/kar/b/1	NG	C			7		>1	40	50
Nam/smi/1/mud	NG		S			ML?	>1	140	290
Nam/kal/1	NG		S		7		>1	120	230
Sa/nam/chi/2	NG	C			7		0.2	170	70
Nam/kd//m/3/1	NG		S		7		0.5	180	110
Man/kar/b/mud/1	NG		?		7		>1	130	360
Nam/smi/sst/1	NG	C	S		7	?	>1	40	90

C - chlorite group; S - smectite group; I - illite group; M - muscovite group; ML - mixed layer; 2nd chlorite peak or kaolinite group.
EAF - East Andaman Flysch; WAF - West Andaman Flysch; NG - Namunagarh Grit.
Note the absence of clay minerals of illite-muscovite groups in NG sandstones and their presence in WAF and EAF sandstones. This possibly is due to presence intermediate-acidic rocks that supplied detritus to the EAF and WAF sandstones and absence of such rocks at the provenance that provides the detritus for NG sandstones. Mixed layer clays (ML) are practically absent in all samples of Paleogene sandstones. Illite crystallinity for EAF and WAF samples are < 1 while for NG samples values are > 1, interpreted as different diagenetic conditions prevailed for the sandstones.

Table 4
Modal compositions of sandstones of West and East Andaman Flysch (from previous page).

Site	Formation	Region	Sample	Q	Total felds	Total Lithic	M	HM	Total
Corbyn's Cove	East Andaman Flysch	S Andaman (South)	FT1B	50.00	18.00	30.00	1.00	1.00	100.00
Corbyn's Cove	East Andaman Flysch	S Andaman (South)	FT3	48.00	28.00	21.00	2.00	1.00	100.00
Corbyn's Cove	East Andaman Flysch	S Andaman (South)	FT4	47.00	19.00	33.00	1.00	0.00	100.00
Brindaban	East Andaman Flysch	S Andaman (Middle)	AND 2	70.00	13.00	3.00	11.00	1.00	100.00
Dundus Point	East Andaman Flysch	S Andaman (Middle)	AND 3	70.00	10.00	11.00	5.00	1.00	100.00
Austin Creek	East Andaman Flysch	Middle Andaman	AND 6	81.00	12.00	6.00	0.00	1.00	100.00
Bandhan Nala	West Andaman Flysch	North Andaman (W coast)	AND 7	67.00	17.00	16.00	0.00	0.00	100.00
Collinpur	West Andaman Flysch	South Andaman (W coast)	AND 1	74.75	10.10	5.05	9.09	1.01	100.00
Rutland	West Andaman Flysch	South Andaman (W coast)	AND 5	76.77	10.10	7.07	2.02	4.04	100.00
Nicobar	West Andaman Flysch	Great Nicobar (E)	AND 8	74.26	13.86	5.94	1.98	3.96	100.00
Nicobar	West Andaman Flysch	Great Nicobar (M)	AND 9	71.72	18.18	8.08	0.00	2.02	100.00
Nicobar	West Andaman Flysch	Great Nicobar (W)	AND 10	66.00	12.00	9.00	12.00	1.00	100.00
Irrawaddy River		Myanmar		52.58	20.62	20.62	3.09	3.09	100.00

Sample	Zircon	Tourmaline	Rutile	Titanite	Apatite	Others	Epidote	Garnet	Chloritoid	Staurolite	Kyanite	Amph	Pyx	Olivine	Spinel	Total	P/F	ZTR
FT1B	4.00	10.67	6.67	4.00	13.33	0.00	24.00	18.67	16.00	0.00	0.00	0.00	0.00	0.00	2.67	100.00	0.27	21.33
FT3	5.71	12.86	7.14	2.86	24.29	4.29	2.86	18.57	17.14	0.00	0.00	0.00	0.00	0.00	4.29	100.00	0.39	25.71
FT4	5.33	12.00	9.33	0.00	14.67	1.33	0.00	20.00	33.33	1.33	0.00	0.00	0.00	0.00	2.67	100.00	0.47	26.67
AND 2	16.43	21.26	5.31	0.00	23.67	0.00	0.00	21.26	7.73	0.00	0.00	0.00	0.00	0.00	4.35	100.00	0.53	43.00
AND 3	7.32	14.63	7.80	1.95	10.73	0.00	3.41	40.00	12.20	0.98	0.00	0.00	0.00	0.00	0.98	100.00	0.61	29.76
AND 6	19.72	16.43	10.33	0.47	15.02	0.00	0.00	19.72	14.55	1.41	0.00	0.00	0.00	0.00	2.35	100.00	0.50	46.48
AND 7	30.69	26.73	7.92	0.00	14.36	1.49	0.00	7.43	3.96	0.00	0.00	0.50	0.00	0.00	6.93	100.00	0.52	65.35
AND 1	6.91	25.35	0.92	2.30	12.44	0.00	18.43	26.27	4.61	1.84	0.00	0.00	0.00	0.00	0.92	100.00	0.56	33.18
AND 5	7.62	3.81	3.33	4.76	5.24	0.00	31.43	35.71	2.38	2.86	2.38	0.00	0.00	0.00	0.48	100.00	0.60	14.76
AND 8	10.78	7.35	1.96	1.47	8.82	0.98	27.94	33.33	3.92	2.45	0.49	0.00	0.00	0.00	0.49	100.00	0.64	20.10
AND 9	8.33	9.80	4.41	4.90	8.33	0.00	28.43	28.92	4.41	2.45	0.00	0.00	0.00	0.00	0.00	100.00	0.55	22.55
AND 10	5.63	20.19	4.23	0.94	11.27	0.00	21.13	22.07	12.21	0.94	0.00	0.00	0.00	0.00	1.41	100.00	0.58	30.05
	2.02	1.01	1.01	2.02	1.01		39.39	7.07	1.01	0.00	0.00	43.43	2.02	0.00	0.00	100.00		4.04

Data source: Allen et al. (2008) and Limonta et al. (2017).
Note the higher content of quartz in WAF compare to EAF and distinctly different abundances of staurolite that provide solid evidence in favour of different provenance of EAF and WAF.

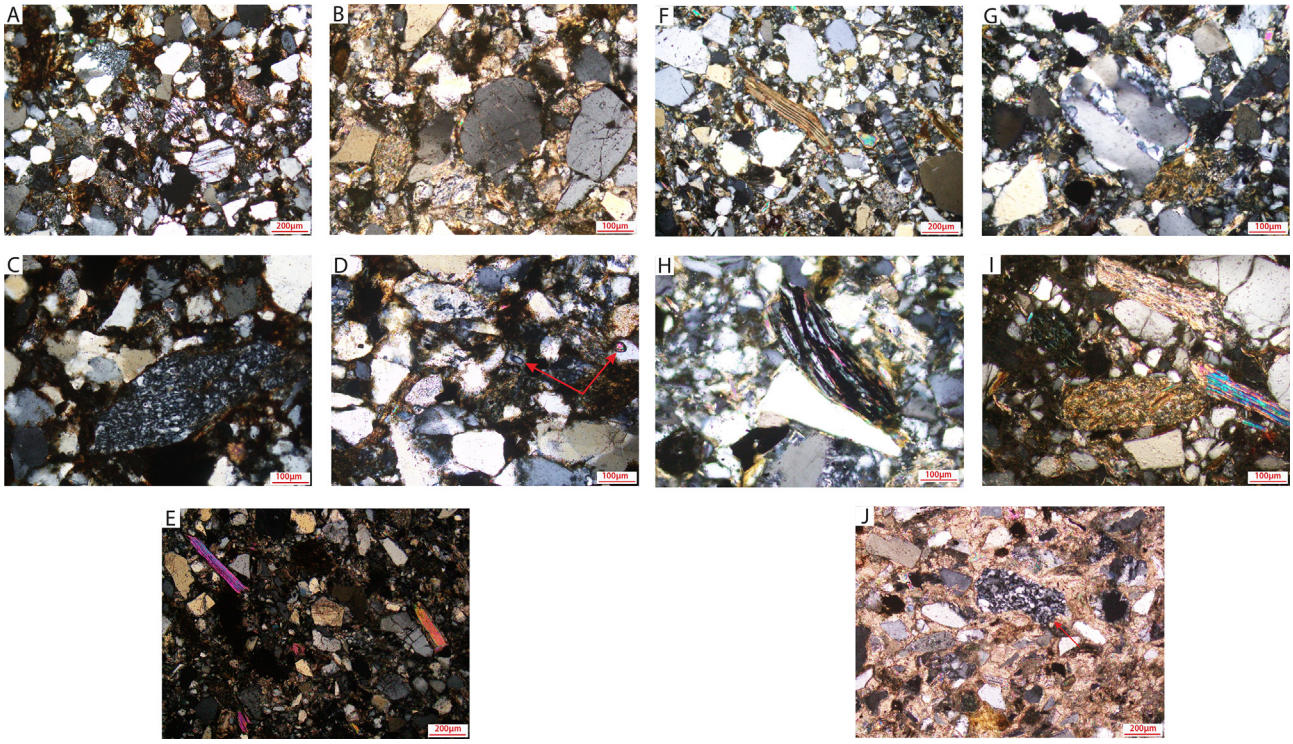

Fig. 8. Photomicrographs of quartz (gray)wackes of East Andaman Flysch (A-E) and West Andaman Flysch (F-J). (A) Medium grained sandstone showing densely packed, angular to sub-rounded, poor to moderately sorted and variably altered framework grains (Mq, Pq, M, Rf) set in a clayey matrix mostly of diagenetic origin (pseudomatrix), Corbyn's Cove, Port Blair. In some thin sections, the matrix makes up to 35 vol% of the rock. (B) Rounded, outsized K-feldspars (RFs) of recycled sedimentary source are conspicuous in the midst of angular and assorted grains, Dundus Point, South Andaman; note the micaschist and quartz-muscovite schist at the bottom of the image. (C) One large, unusual spindle shaped chert grain of suspected volcanic origin; the surrounding groundmass exhibits medium to finer grain size and mostly angular to subrounded quartz and feldspar. (D) An illustration of typical (gray)wacke from East Andaman Flysch, North Bay, SA; small and well-rounded zircon grains (arrowed) indicate a sedimentary provenance. (E) East Andaman Flysch sandstone showing crude schistose texture defined by parallel orientation of framework grains including muscovite flakes. (F) Rarely preserved unaltered biotite flakes and slender crystal of plagioclase in West Andaman Flysch. (G) Highly assorted and angular to rounded framework grains in West Andaman Flysch sandstone at the middle of the photograph showing outsized and strained polycrystalline quartz, indicating a metamorphic provenance and local transport. (H) West Andaman Flysch sandstone showing a schist fragment in the middle of the micrograph; quartz grains are stretched, elongated, and have undulose extinction, revealing a medium to high rank metamorphic source, Great Nicobar Island. (I) Various lithic grains in West Andaman Flysch from Great Nicobar Island. (J) Typical carbonate cemented sandstone of WAF, Bandhan nala, NA. All micrographs are in XPL.

(Cullers et al., 1988). The Th/U ratio (2.5–4.5, average 2.9) for NG sandstones are less than that of upper crustal igneous values (3.5–4.0; (McLennan et al., 1993). Such values are similar to a depleted mantle source indicating input from young differentiated magmatic arc (Girty et al., 1994; McLennan et al., 1993). The Th/Sc ratio (Av. 0.13) (Supplementary Table 1) imply input from endogenic processes that is consistent with strong petrographic signature of juvenile grains in sandstones. The Th/Sc ratio is < 0.05 in Namunagarh Grit sandstones are lower than crustal value (~0.50) (McLennan et al., 1990). The grit samples show moderate negative to small positive Eu anomalies (Eu/Eu^{*}= 0.70–1.24), confirming mafic parent rocks (Clift et al., 2008). There is a large contrast in total REE (ΣREE) concentrations between the sandstones of Namunagarh Grit and Andaman Flysch. In Namunagarh Grit sandstones, ΣREE contents are generally < 130 ppm. To provide robust constraints on the nature and intensity of weathering and parent rock composition for NG and Flysch sandstones/mudstones were determined using different indexes: Chemical Index of Alteration (CIA) (Nesbitt and Young, 1982; 1984); Chemical Index of Weathering (CIW) (Nesbitt and Young, 1982); Vogt Ratio (V) (Roaldset, 1972; Vogt, 1927); Weathering Index Potential (WIP) (Parker, 1970); Index of Compositional Variability (ICV) (Cox et al., 1995) values (Supplementary Table 1). The trend of weathering pattern was determined by plotting concentration of Al_2O_3, Na_2O and K_2O on ternary diagram of (Nesbitt and Young, 1982; Nesbitt and Young, 1984). The CIA and the ICV values are frequently used to trace the parent rocks and provenance of sediments (Bhat and Ghosh, 2001; Cullers and Podkovyrov, 2000; Joo et al., 2005). Matured sediments derived from the stable continental crust display low ICV values (<1.0), whereas immature sediments from arc-related volcanic and plutonic rocks exhibit high values. ICV Values for sandstones (Av. 1.24) and mudstones (Av. 1.11) of the Namunagarh Grit reflect immature parent rocks.

So, the key geochemical characteristics collectively suggest rocks of intermediate composition (andesite) were the major source of sediments for Namunagarh Grit sandstones, alongside a minor to subordinate input from rocks of felsic composition. The parent rocks experienced insignificant chemical weathering and significant physical weathering during Namunagarh Grit sedimentation and suggest proximal location of the source terrane.

East Andaman Flysch sandstones with an average 71.5 wt% SiO_2 and the K_2O/Na_2O ratio ≤ 1 (Supplementary Table 1), is similar to sandstones that are of quartz-intermediate type (Crook, 1974) deposited in an active continental margin (Andean-type) tectonic setting and received sediments from basement. Two sandstone samples with high (>80 wt%) SiO_2 and low (<10 wt%) Al_2O_3 (Supplementary Table 1) reflect their quartz arenite composition and texture (Condie, 1993). These two samples have ICV values 0.80 and 0.91 that support a source made of stable continental crust. The interbedded mudstones have average ICV value 0.74 indicating derivation from a cratonic environment where recycling and weathering processes predominated. The previous geochemical study of East Andaman Flysch from Corbyn's Cove also revealed compositional range falls within the intermediate type

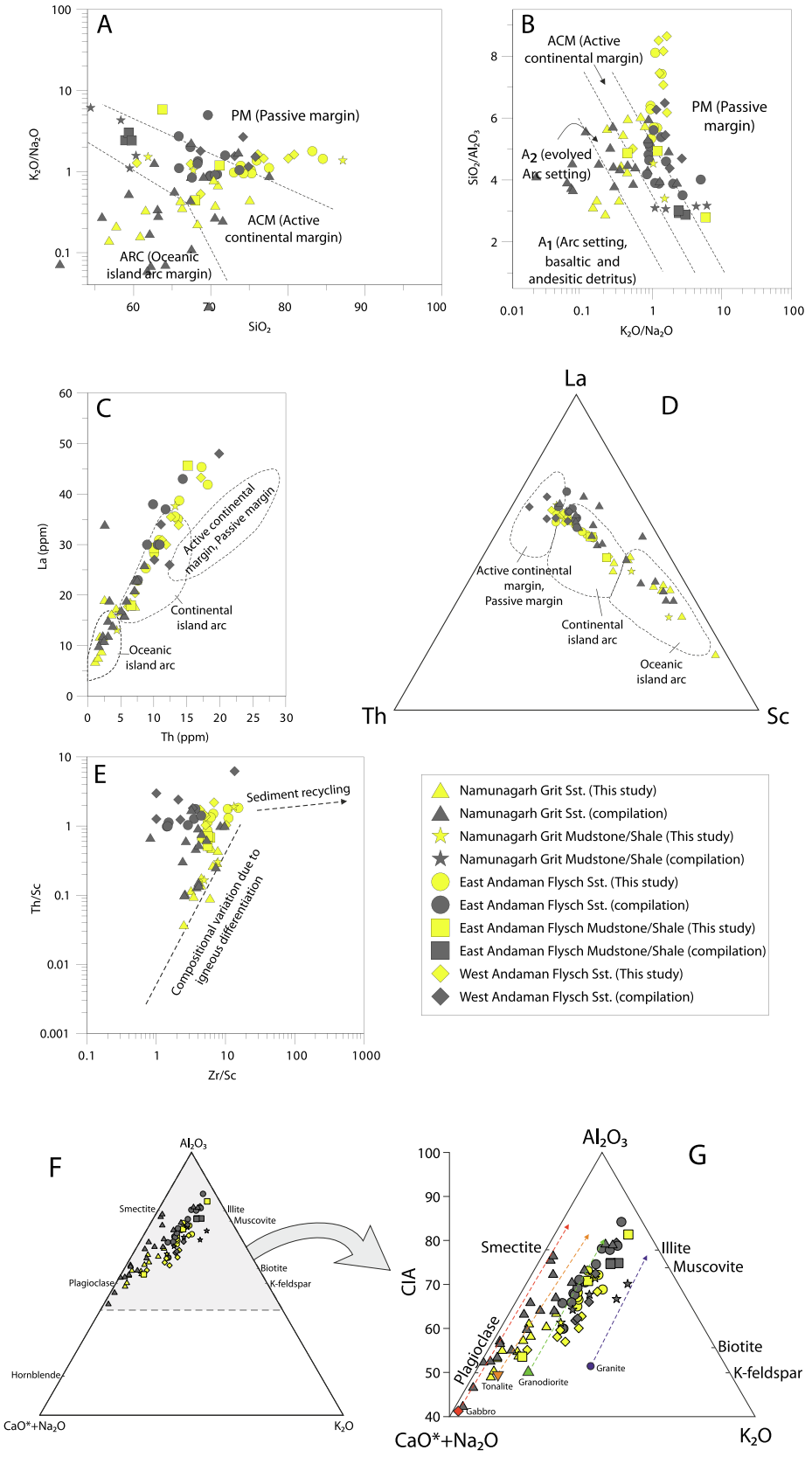
A
PM (Passive margin)
ACM (Active continental margin)
ARC (Oceanic island arc margin)
K2O/Na2O
SiO2
B
ACM (Active continental margin)
PM (Passive margin)
A2 (evolved Arc setting)
A1 (Arc setting, basaltic and andesitic detritus)
SiO2/Al2O3
K2O/Na2O
C
Active continental margin, Passive margin
Continental island arc
Oceanic island arc
La (ppm)
Th (ppm)
D
La
Th
Sc
Active continental margin, Passive margin
Continental island arc
Oceanic island arc
E
Sediment recycling
Compositional variation due to igneous differentiation
Th/Sc
Zr/Sc
Namunagarh Grit Sst. (This study)
Namunagarh Grit Sst. (compilation)
Namunagarh Grit Mudstone/Shale (This study)
Namunagarh Grit Mudstone/Shale (compilation)
East Andaman Flysch Sst. (This study)
East Andaman Flysch Sst. (compilation)
East Andaman Flysch Mudstone/Shale (This study)
East Andaman Flysch Mudstone/Shale (compilation)
West Andaman Flysch Sst. (This study)
West Andaman Flysch Sst. (compilation)
F
Al2O3
Smectite
Illite
Muscovite
Biotite
K-feldspar
Plagioclase
Hornblende
CaO*+Na2O
K2O
G
Al2O3
CIA
Smectite
Illite
Muscovite
Biotite
K-feldspar
Plagioclase
Granite
Granodiorite
Tonalite
Gabbro
CaO*+Na2O
K2O

(Bandopadhyay and Ghosh, 2015). The SiO_2/Al_2O_3 ratio determines the compositional maturity of sediments (Armstrong-Altrin et al., 2012; 2013; Etemad-Saeed et al., 2011; Madhavaraju, 2015). The Si/Al average ratio in basic igneous rocks is 3, whereas it is about 5 in the acid igneous rocks, hence the values > 5 in clastic sediments indicate sediment maturity (Roser et al., 1996). The ratios in the East Andaman Flysch (Av. 5.9) and Al_2O_3/TiO_2 ratios considered to reflect parent rock compositions, in mafic igneous rocks (SiO_2 content from 45 to 52 wt%) range from 3 to 8, in intermediate rocks (SiO_2 content from 53 to 66 wt%) from 8 to 21, and in felsic rocks (SiO_2 from 67 to 76 wt%) from 21 to 70 (Hayashi et al., 1997; Willis et al., 1988). East Andaman Flysch sandstones have an average Al_2O_3/TiO_2 ratio of 15.0. These values indicate intermediate type parent rocks either due to direct contributions from Precambrian sediments that typically show ratios between 15 and 25 or mixing of sediments from both mafic and felsic type sources. Subtle variations between the East and West Andaman Flysch also follow from major oxide plots in sandstone classification diagrams of Herron (1988) and Pettijohn et al. (1972), with the East Andaman Flysch showing dominantly lithic arenite to (gray)wacke composition, whereas West Andaman Flysch plot closer to the arkose field within the lithic arenite field. The geochemistry of the Great Nicobar sandstones is closer to the West than to the East Andaman Flysch (Supplementary Table 1), consistent with the higher petrographic similarity. On a SiO_2 versus K_2O/Na_2O diagram of Roser and Korsch (1986) the majority of the East Andaman Flysch sandstones fall within the active continental margin field (Fig. 9A). The range and average concentration of major elements of interbedded mudstones (Supplementary Table 1) when compared with mudstones of continental arc, back arc, and forearc basins (McLennan et al., 1990), the average composition of mudstones lies close to that of a continental arc basin (Long et al., 2008).

West Andaman Flysch samples with consistently higher K_2O content than Na_2O (Supplementary Table 1) reflect the arkosic composition of the sandstones suggesting a granitic source (Pettijohn, 1963). Average P/F ratios (0.56) for West Andaman Flysch samples are higher than the 0.45 for the East Andaman Flysch. This contrast reflects increasing presence of granodiorite in the source of East Andaman Flysch. Chemical data of the West Andaman Flysch and Greater Nicobar sandstones in tectonic discrimination diagrams mostly plot on the Passive Margin tectonic field, while East and West Andaman Flysch data largely plot in the active margin Island Arc field (Fig. 9A-D). The Zr/Th ratio of East Andaman Flysch confirm that these sandstones are arc-derived and in all probability that the arc bears characteristics of both continental and oceanic arcs. Sandstones of the East Andaman Flysch show Cr enrichment (97.44–164.79 ppm, av. 113.46 ppm) likely derived from chrome spinel in ultramafic rocks. High Rb concentrations (>40 ppm) and low Rb/Sr (0.04–3.24) ratios are indicative of felsic to intermediate igneous sources that have undergone weak chemical weathering (Long et al., 2008). High Rb/Sr values have been interpreted as a signature of strong weathering and sedimentary recycling (McLennan et al., 1993). In comparison, the average Rb/Sr values (Supplementary Table 1) in the studied sandstones and mudstones are lower. The Th/Sc values (Supplementary Table 1) are indicative of derivation of detritus from old differentiated upper continental crust (McLennan et al., 1990; McLennan, 1989). The Th/Yb ratios in East and West Andaman Flysch sandstones (Supplementary Table 1) are higher than that of PAAS (Post Achaean Australian shale) (5.21) indicating that granitic clastic materials are more silicic than the average granodiorite (Lee, 2009). West Andaman Flysch sandstones (7.2) reflect that they are more mature than East Andaman Flysch, corroborated by the occurrence of fewer lithic grains in the West Andaman Flysch. Two analyses (Supplementary Table 1) of the West Andaman Flysch sandstones showed high $CaCO_3$ concentrations. These do not reflect provenance, but rather represent a carbonate cement confirmed by petrographic observations.

Upper continental crust (after Rudnick and Gao, 2014) normalized trace element (Fig. 10A-E) and Chondrite (after Sun and McDonough, 1989) normalized (Fig. 10F-J) REE distribution pattern is flat in all samples and LREE are enriched relative to HREE. ΣREE contents in the Andaman Flysch vary from 115 to 340 ppm. Compared to the Namunagarh Grit samples, the Andaman Flysch rocks have much higher light REE abundances (La_N/Sm_N = 2.7–5.2). In general, the patterns resemble those of Upper Continental Crust and PAAS and the Andaman Flysch samples plot closer to PAAS implying derivation of detritus from upper continental crust. Eu anomalies (Taylor and McLennan, 1985) show negative values in all samples (Eu/Eu^*= 0.49–0.75) suggesting intracrustal fractionation of plagioclase.

Finally, the ICV for East Andaman Flysch ranges between 0.87 and 1.33 (av. 1.11) while it is between 0.92 and 1.27 (av.1.11) for West Andaman Flysch. The average values, being just marginally higher than 1.0 imply that the parent rocks were moderately mature, which in turn indicates that the sandstones underwent moderate recycling processes.

Fig. 9. Tectonic setting discrimination diagrams based on major and trace elements for Namunagarh Grit, East Andaman Flysch and West Andaman Flysch sandstones. A) K_2O/Na_2O-SiO_2 diagram (after Roser and Korsch, 1986) showing data for NG sandstones plot on arc and ACM fields; data for East Andaman Flysch straddling along the line dividing the ACM and PM fields while most of the WAF sandstones data plot on PM field where granite is the dominant rock types. B) SiO_2/Al_2O_3-K_2O/Na_2O diagram (after Roser and Korsch, 1986; A_1 = Arc setting, basalt and andesitic detritus, A_2 = Evolved arc setting, felsic-plutonic detritus). NG sandstones predominantly plot on A_1 and A_2 fields while a few data plot on ACM fields. West Andaman Flysch sandstones largely occupy the PM field while the EAF sandstones predominantly plot on ACM field and a few on PM fields. Trace elements based Th-La (C) and La-Sc-Th (D) discrimination diagrams (after Bhatia and Crook, 1986) showing good discrimination in tectonic settings. Note that the ACM and Passive Margin fields are indistinguishable in these diagrams. In Th-La bivariant diagram (C) Namunagarh Grit sandstones plot in oceanic island arc setting dominated by basalt while East Andaman Flysch data plot in a fairly narrow region on Continental Island Arc field dominated by granodiorite. West Andaman Flysch sandstones mostly plot on the passive margin field where granite predominates. La-Sc-Th triangular plots (D) show excellent discrimination of turbidites of the Andaman Nicobar Accretionary Ridge; all Namunagarh Grit sandstones and mudstones plot, spread over the oceanic island arc field with a tendency towards Continental Island arc while majority of the East Andaman Flysch and West Andaman Flysch data plot on Continental Island Arc and a few on ACM/PM fields where granitic and gneissic rocks predominate. Note the distinct plot of three Namunagarh Grit mudstone samples very close to andesite. E) Binary scatter plot (Th/Sc versus Zr/Sc, McLennan et al., 1993) used to determine mafic and felsic contribution and possible recycling processes. Plots indicate mafic to felsic volcanic rocks as sources for Namunagarh Grit and upper crustal granite and granodiorite sources for West Andaman Flysch and East Andaman Flysch. Sediment recycling indicated by addition of zircon (McLennan et al, 1993) appears negligible in Paleogene clastic sediments of Andaman Nicobar Accretionary Ridge. F) Ternary plot of molecular proportions of Al_2O_3- (CaO^* + Na_2O)- K_2O for Paleogene turbiditic sandstones and mudstones of the Andaman-Nicobar Islands (after Nesbitt and Young, 1982). Most samples plot between plagioclase and average shale, suggesting a low to moderate weathering at the provenance. G) CIA on the left is Chemical Index of Alteration. Ideal weathering trend (IWT) is given by dashed line parallel to the A–CN. Note that weathering trend for NG sandstones can be traced back to the gabbro-tonalite parent lithology while both West Andaman Flysch & East Andaman Flysch sandstones meet the granodiorite- granite composition. These trends imply that the turbiditic sandstones underwent a little post-depositional K-metasomatism. CIA values range from 50 for fresh primary igneous rocks to a maximum of 100 for the most weathered rocks (Fedo et al., 1995). Data for tonalite (To), granodiorite (Gd), granite (Gr), and average Archean upper crust are from Condie (1993).

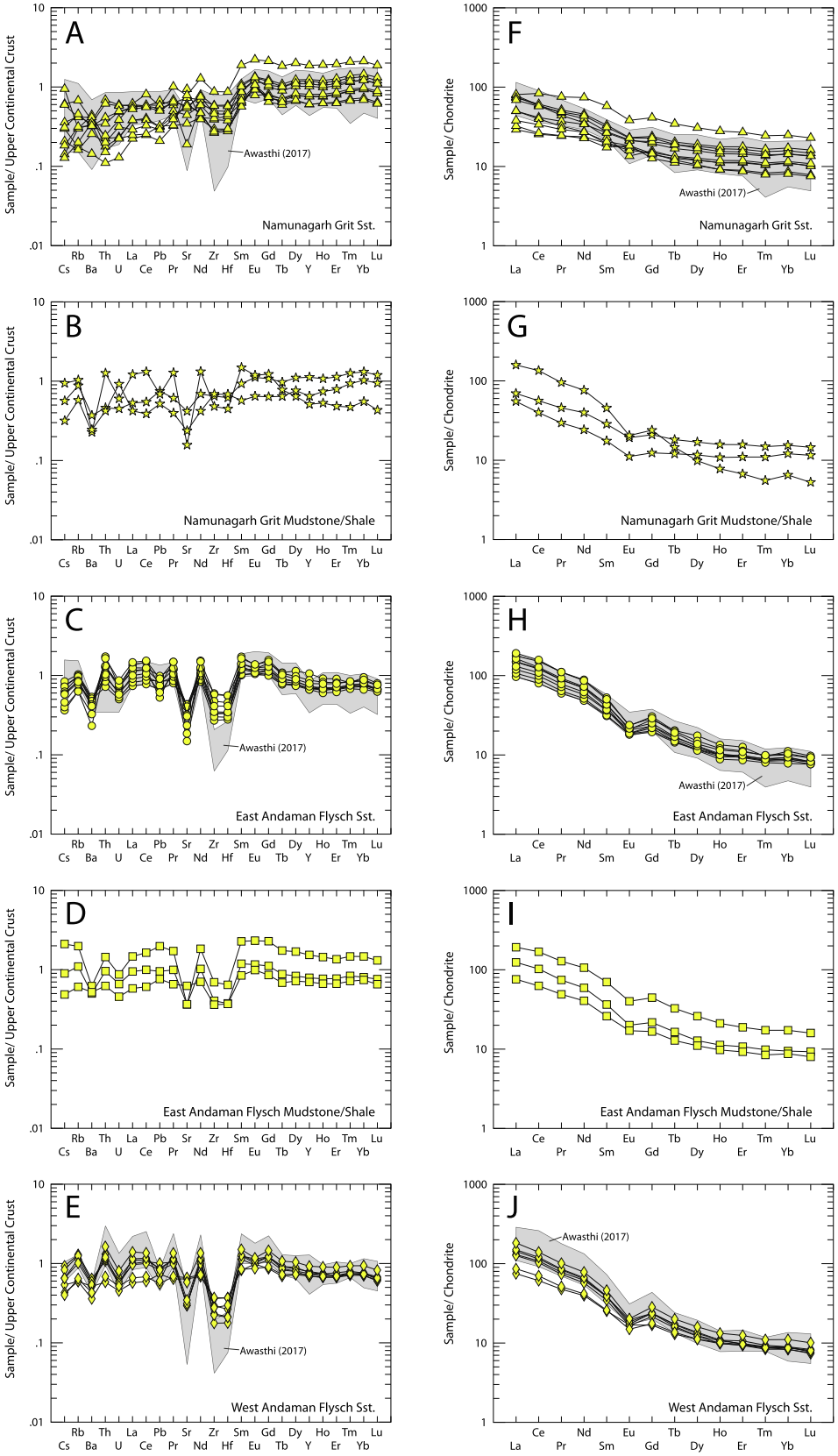

Fig. 10. Upper Continental Crust (UCC, after Rudnick and Gao, 2014) -normalized trace element patterns for sandstones and mudstones (fine mudstone/siltstone) of the Namunagarh Grit (A-B), East Andaman Flysch (C-D) and West Andaman Flysch (E), and Chondrite (after Sun and McDonough, 1989) -normalized REE patterns for the same rock types (F-J). Grey shaded regions represent corresponding compositional spectrum (reinterpreted in this study based on location) after Awasthi (2017).

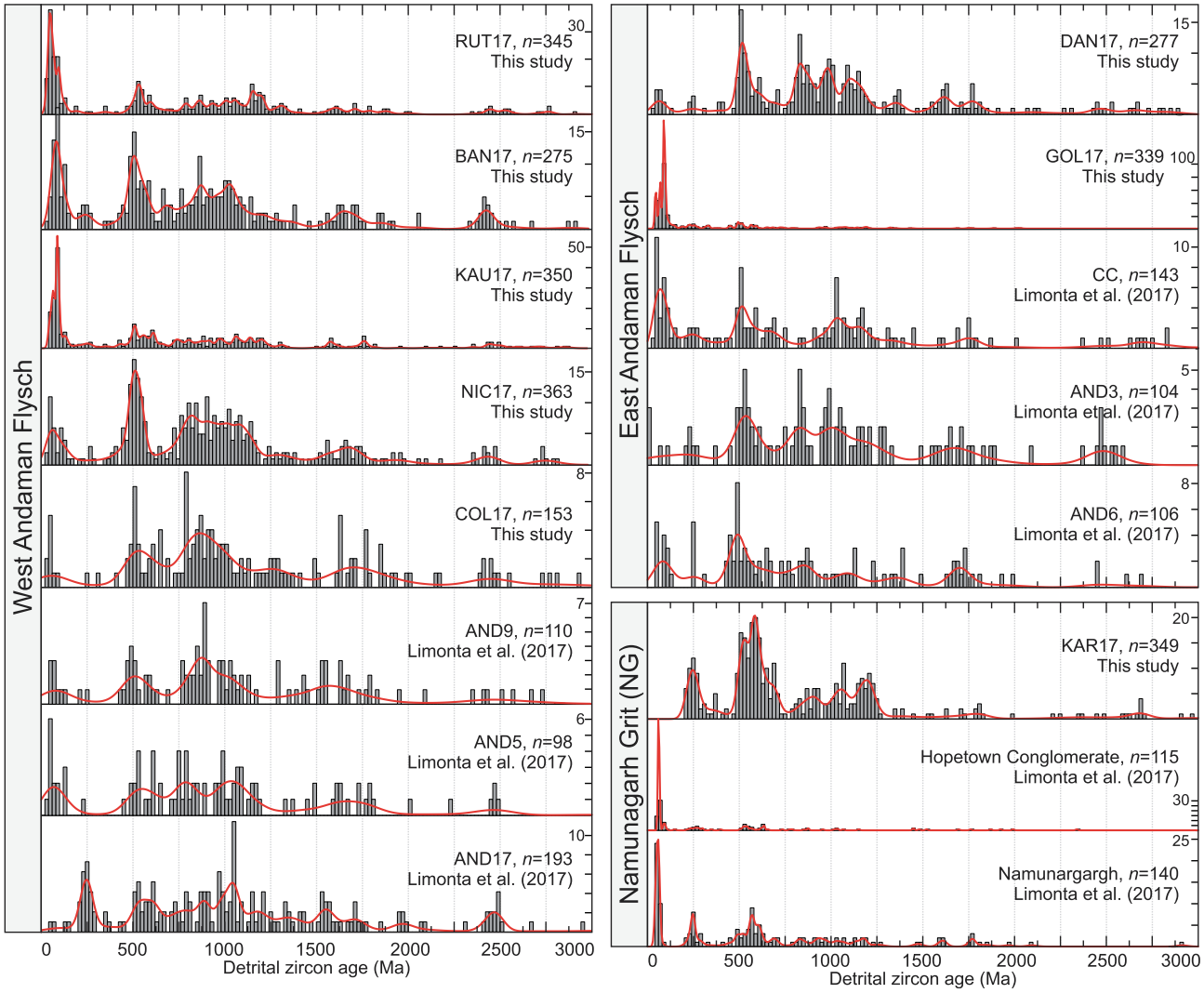

Fig. 11. Histograms and kernel density estimate diagrams for detrital zircon age distributions from the Namunagarh Grit, East Andaman Flysch, and West Andaman Flysch (this study and Limonta et al., 2017). All ages are displayed in 20 Ma bins; number on y axis is the amount of zircon age per bin. Three NG samples from the Kalipur coast (2) and Mungleton (1) from Bandopadhyay and Carter (2017a) are not displayed because of low zircon number (n < 80).

4.3. U-Pb geochronology

Individual age distributions are displayed in Fig. 11; compiled age distributions are displayed in Fig. 12 and compared with compilations from neighbouring basins (Bengal Bay, central Myanmar, and Sumatra). Samples from the West Andaman Flysch share several large age populations at 30–100 Ma, 480–1400 Ma with peaks at 510 Ma, 870 or 1050 Ma, 1520–2000 Ma, and 2350–2590 Ma with a peak at 2450 Ma (Fig. 11). The contribution of the late Cretaceous – Paleogene, 30–100 Ma age population is prominent in samples RUT17, BAN17 and KAU17, and minor in other samples; this population displays three main age peaks at 45 Ma, 70 Ma and 95 Ma. Three samples (BAN17, NIC17, and AND17) display a well-marked age population at 180–300 Ma, which is barely expressed in other samples (Fig. 11).

Samples from the East Andaman flysch display the same inter-sample variability and the same age populations (including three well-marked age peak at 50, 70 and 95 Ma) except for the 2350–2590 Ma age population that is only clearly observable in one sample (AND3, Limonta et al., 2017). Sample GOL17 displays a dominant Late Cretaceous – Paleogene age population, while most others have dominant contributions of Precambrian ages.

Samples from the Namunagarh Grit samples display a high variability in age distributions; sample KAR17 (this study) is completely devoid of late Cretaceous – Paleogene zircons, while samples from the Hopetown Conglomerate, Namunargarh (Limonta et al., 2017), Kalipur Coast, and Mungleton Quarry (Bandopadhyay and Carter, 2017a) are dominated by 30–100 Ma ages, with a prominent 60 Ma peak, which is absent in the West and East Andaman Flysch. Samples KAR17 and Namunargarh have particularly well-expressed 180–300 Ma age populations; the 2350–2590 age population is absent in all samples.

There is no clear difference between the maximum depositional ages and youngest zircon ages for samples of the East and West Andaman flysch (Table 2). Youngest zircon ages reach the early Miocene (23.1 ± 1.2 Ma for the West Andaman Flysch, 18.7 ± 1.4 Ma for the East Andaman Flysch), though youngest age populations with three or more overlapping ages are commonly Eocene (50 to 40 Ma). These youngest ages are somewhat younger than the previous, poorly constrained age assignment of Oligocene, and are consistently older than the oldest ages of ~18 Ma estimated for the overlying Archipelago Group (Awasthi and Ray, 2020). Our Namunagarh Grit sample (KAR17) yielded a maximum depositional age of > 200 Ma, considerably older than the Paleogene

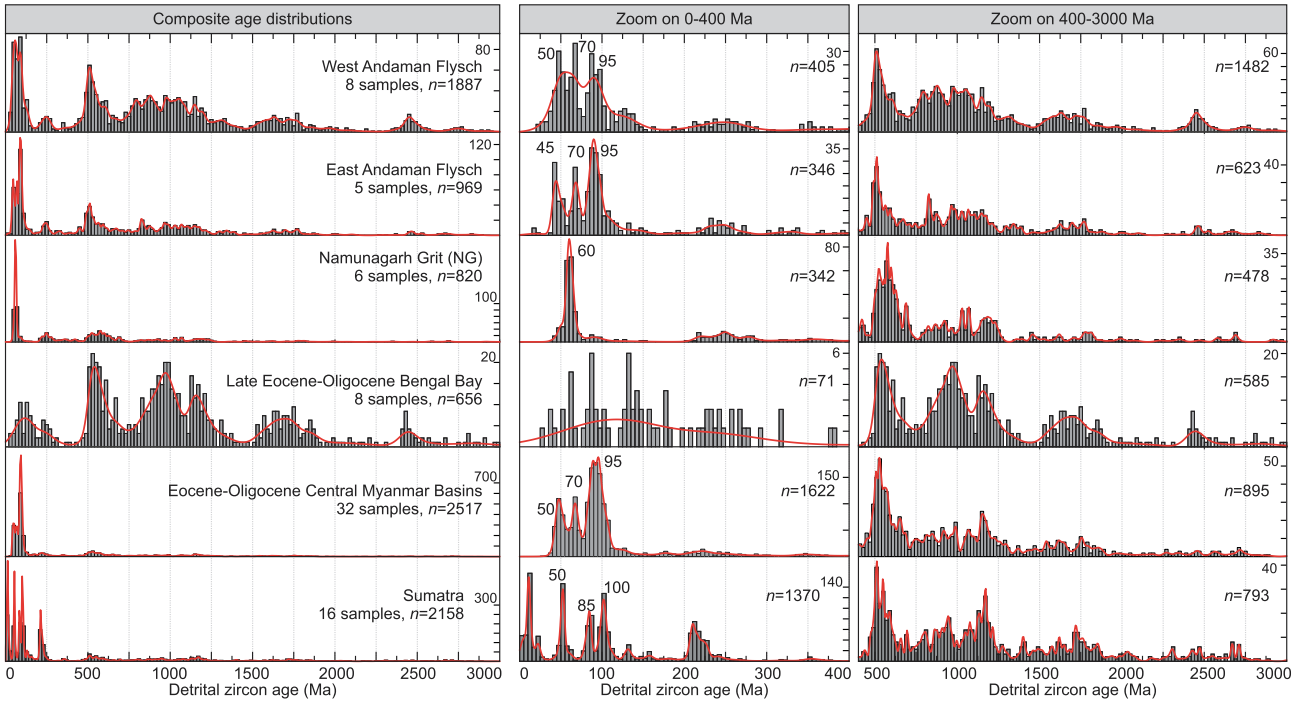

Fig. 12. Histograms and kernel density estimate diagrams for sample groups for the Namunagarh Grit, East and West Andaman Flysch (samples on Fig. 11), compared to compilations from central Myanmar (Eocene and Oligocene sandstones; Cai et al., 2020; Licht et al., 2019; Morley and Arboit, 2019; Oo et al., 2015; Robinson et al., 2014; Wang et al., 2014; Arboit et al., 2021), Sumatra (Zhang et al., 2019), and the Bengal Bay (Eocene to Oligocene Barail Formation; Bracciali et al., 2015; Vadlamani et al., 2015; Yang et al., 2019). All ages are displayed in 20 Ma bins (0 to 3000 Ma, 400 to 3000 Ma) and 5 Ma bins (0 to 3000 Ma); number on y axis is the amount of zircon age per bin.

age that follows from biostratigraphy, and this sample thus does not further constrain the age of the formation.

5. Discussion

5.1. Provenance of the Namunagarh Grit formation

Combined paleocurrent, petrographic, geochemical, and geochronological data suggest that the Namunagarh Grit contains abundant sediment from nearby pyroclastic eruptions of andesitic arc volcanoes. The tuffaceous sandstones record contributions from post-eruptive erosion of volcanoes and a dissected/transitional arc; the age distribution of sample KAR17 illustrates the presence of a secondary source devoid of contemporary magmatism exposing older continental basement (Fig. 11). If the variable paleocurrent directions measured in the Namunagarh Grit sandstones are primary and not dispersed due to later tectonic deformation, the contributions of sediments to the shallow-water forearc were derived from east, west, north, and south. Contributions from north, south, and east would point to a Sunda arc and forearc provenance, including continental basement of West Sumatra and the rest of Sundaland, as well as from the Woyla Arc. A derivation from the west, however, is puzzling in modern geography, as to the west of the Andaman Islands is the Sunda Trench today. However, with paleomagnetic data suggesting that the paleolatitude of the West-Burma Block in Late Cretaceous to Eocene time was similar as Sumatra (Westerweel et al., 2019), it is possible that this block, or arc rocks associated with subduction below the West Burma Block, formed a source from the west, rather than the north of the Andaman Islands.

A puzzle provided by our detrital zircon results combined with previously published data is the age peak in the Namunagarh Grit at 60 Ma. This age peak does not exist in Sumatran sandstones (Zhang et al., 2019), but also not in in the central Myanmar Basin where instead an age peak of 70–80 Ma is prominent (Fig. 12; Cai et al., 2020; Licht et al., 2019; Morley and Arboit, 2019; Oo et al., 2015; Robinson et al., 2014; Wang et al., 2014). The origin of the 70–80 Ma age population remains debated, as no latest Cretaceous plutons have been found in the Wuntho-Popa Arc that formed on the West Burma Block, associated with the subduction along its modern western, but paleogeographically southern margin (Licht et al., 2020). Westerweel et al. (2020) speculated about an origin in northern Myanmar for these zircons, at the southern edge of the Himalayan syntaxis, exhumed by the indentation of the Indian Plate along the northern Myanmar subduction margin. Our results clearly show that a 60 Ma volcanic source must have come proximal to the Andaman Islands to deliver the Namunagarh Grit sediments. It is not feasible that these were derived from the eastern Himalaya. We thus tentatively suggest that in Late Cretaceous time, the Wuntho-Popa volcanic arc migrated inland from the West Burma trench, to disappear off the northern (present-day eastern) West Burma margin to an intra-oceanic position by 60 Ma (Fig. 13). The original northern (present-day eastern) margin and the adjacent oceanic lithosphere of the West Burma has been underthrusted first below the Andaman forearc and later below the Shan Scarp. By 80–70 Ma, the arc would then still have been able to shed sediments to the Central Myanmar Basin, whilst by 60 Ma it was too far offshore (similar to Barren Island today east of the Andaman Islands). The arrival of the 60 Ma arc in the trench below Andaman would then provide the source for the Namunagarh Grit formation. Undated arc-related agglomerates that are found associated with melanges below the Andaman Ophiolites (e.g., Bandyopadhyay et al., 2021) may represent relics of this arc, and relics may be found in the melanges along the Sagaing fault along the eastern West Burma Block (e.g., Lai et al., 2018). Future work on these complexes may shed further light on the enigmatic 80–60 Ma arc of which relics are found in Myanmar and Andaman – for now we conclude that the gap in arc magmatism in Myanmar between Cretaceous and Eocene time (Licht et al., 2020) may

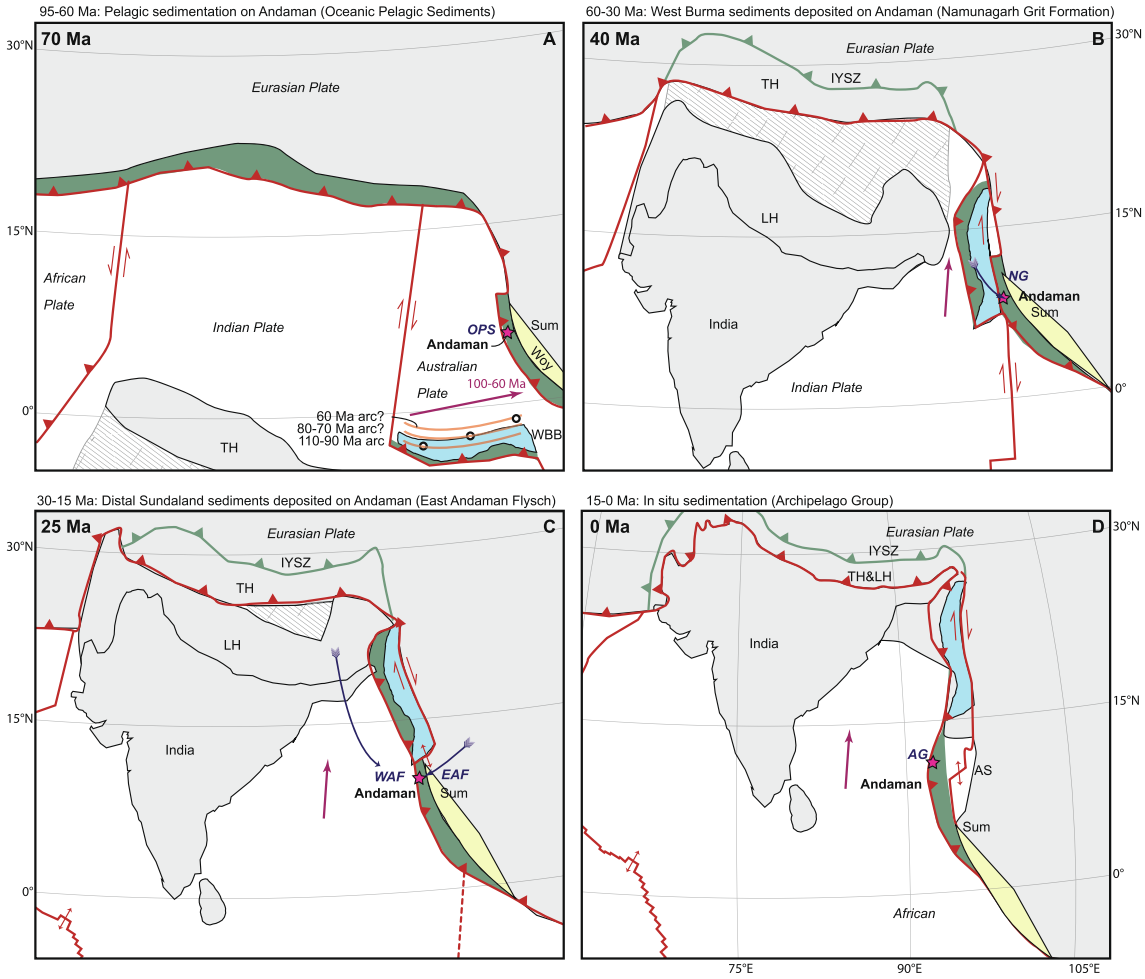

Fig. 13. Paleogeographic scenario for the eastern Neotethys Ocean. Reconstructions are cast in a paleomagnetic reference frame (Torsvik et al., 2012), using reconstructions of Asian deformation and India-Asia motion as detailed in van Hinsbergen et al. (2011a; 2019) and Advokaat et al. (2018b). See text for further explanation.

reflect a relocation rather than a temporal termination of arc magmatism.

Contribution of sediment from a volcanic arc is also supported by the wide variation in $(La/Yb)_N$ ratios from 3.52 to 9.54 (Av. 5.28) in Namunagarh Grit sandstones, suggesting that sediments were derived from more than one common source and that mixing was not very efficient during transport and deposition (Lee, 2009). The Al_2O_3/TiO_2 ratios indicate contribution from dominantly andesite but ranging to rhyodacite. Presence of mafic parent rocks is indicated by Th/U ratio (Av. 2.92) and the elevated concentration of Cr and Ni in Namunagarh Grit sandstones also indicates ultramafic material exposed in the source region. Ultramafic rocks of the Andaman ophiolites may be present in the source area, but given that these form the basin floor, this is not likely. Instead, the ophiolites of surrounding the West Burma Block may be a more likely candidate. Finally, the CIA of Namunagarh Grit sandstones, ranging from 49.21 to 60.60 (Av. 56.25), is consistent with incipient weathering at the provenance region. The low CIA may be due to faster rate of physical weathering than chemical one during sedimentation of the Namunagarh Grit which in turn imply rapid uplift and associated denudation (physical erosion, Garzanti and Resentini, 2016) instead of chemical weathering of rocks of the provenance region. ICV > 1.0 indicate low mineralogical maturity and first cycle sediments with little recycling; Observed CIA and the ICV values both higher than that of PAAS suggest that the provenance region experienced weak chemical weathering and the detritus were mainly derived from an immature source.

In summary, the source of the Namunagarh Grit sandstones contained an active, 60 Ma volcanic arc, as well as detritus from deeper crustal level exhumed and eroded during maturation of the arc. The Namunagarh Grit was deposited in shallow water but overlies an ocean floor and pelagic and hemipelagic sediments. Combined, the deepwater Andaman forearc must have been uplifted by several kilometres in the early Paleogene, and in the process must have converged with a continental arc. While there may be a contribution of the Woyla Arc to the east, the proximity of also a continental source, an active arc, and ophiolites, may indicate that the uplift of the Andaman forearc may be caused by the eastward underthrusting of the West Burma Block, and likely a volcanic arc in the ocean to its north, below the Andaman forearc (Fig. 13).

5.2. Provenance of the East and West Andaman Flysch: Are they the same stratigraphic unit?

Despite similarities in zircon age distributions, there are recognizable differences between the East and West Andaman Flysch that suggest differences in the contribution of their source areas. Sandstone modal analyses data give higher quartz content, but lower total feldspar and lithic grains for the West than the East

Andaman Flysch sandstones, while the latter are richer in volcanic grains (Table 4). Staurolite and garnet, common in Himalaya-derived sediments, are present in almost all samples of the West Andaman Flysch and Great Nicobar Flysch, but virtually absent in the East Andaman Flysch (Table 4). Our geochemical data suggest that the East Andaman Flysch was likely derived from an active continental margin. The West Andaman and Great Nicobar Flysch sandstones indicate a matured crustal source dominated by granitic rocks and deposition on a passive margin tectonic setting while the East Andaman Flysch sandstones were derived from continental sources rich in granitoid rocks and in minor quantity from volcanic arc (Fig. 9B, C, D).

Importantly, both the East and West Andaman Flysch display Cretaceous-Cenozoic age populations that are identical to those of coeval Burmese sediments, with three well marked populations at 35–50, 70–80, and 90–100 Ma that are not found elsewhere in the area (Fig. 12). West Andaman flysch samples only differ by having a well-marked age population at 2350–2590 Ma (Fig. 12), only found in Bengal Bay, Bengal Fan and Nicobar Fan samples (McNeill et al., 2017; Chen et al., 2020; Pickering et al., 2020). Collectively, the sediment provenance data suggest that the East Andaman Flysch, which was deposited on the Andaman ophiolites in the forearc of the Sunda trench, was derived from the West Burma Block, with likely additional supply from Sundaland. The West Andaman Flysch, on the other hand, likely display an additional supply derived from the India-Asia collision zone, probably alongside trench fill sediments that share a provenance with the East Andaman Flysch, and form an accretionary prism scraped from subducted Indian plate lithosphere.

Our analysis thus suggests that the Namunagarh Grit, the East, and the West Andaman Flysch likely received sediments from the West Burma Block. The interpreted proximity, paleobathymetry, and sediment contributions of the three units are yet strongly different. The deposition of the Namunagarh Grit and the Andaman Flysch are separated by a phase of major subsidence; sediment sources for the Andaman Flysch were much more distal, and the contributions of a clastic continental source compared to a volcanic arc source were strongly increased. This suggests that the West Burma Block that was proximal during deposition of the Namunagarh Grit either subsided—for which there is no evidence in Myanmar—or moved away from the Andaman Islands. In addition, the distal continental sediment source that started to contribute to the sediments on the Andaman Islands was, given the sediment composition, the position in the forearc of the Sunda Trench, and the U–Pb detrital zircon age spectra, probably not the India-Asia collision zone. Instead, this may have been the Sundaland core east of the Andaman Sea.

5.3. Implications for the Cenozoic paleogeography and plate tectonic evolution of the eastern Neotethys and West Burma Block

The stratigraphy and sedimentology of the Andaman Islands reveals four distinct tectonic intervals that are helpful in constraining the paleogeography of the eastern Neotethyan realm. After the initiation of subduction below the Andaman Ophiolites, around 105 Ma (Bandyopadhyay et al., 2021; Plunder et al., 2020), and a 98–93 Ma interval of arc magmatism, the Andaman Ophiolites were the site of (hemi-)pelagic, deep water, oceanic sedimentation until the latest Cretaceous, beyond reach of significant clastic sediment input, but within reach of occasional arc-derived ashes (Jafri et al., 1993). This changed in the 60–40 Ma interval, when the Andaman ophiolites became uplifted, probably by several kilometres, to shallow-water conditions during which the Namunagarh Grit was deposited. Whilst the uplift, and likely some of the shortening that affected the Andaman Islands, may have brought sediments from the Woyla Arc of North Sumatra within reach, our sediment provenance data suggest that this event involved the juxtaposition of the West Burma Block and the Andaman Islands.

In Fig. 13, we provide snapshots of a kinematic reconstruction of West Burma relative to Sundaland to illustrate how the mobilist view on the West Burma Block of Westerweel et al. (2019) provides an avenue to explain the sediment provenance history of the Andaman Islands that we documented in this paper. We made a subtle modification of the model of Westerweel et al. (2019): those authors placed the West Burma Block at 95 Ma at the average paleolatitude constrained from granitoids in the West Burma Block of ~8°S (their Fig. 4). In our reconstruction, we use a plate kinematic approach. Constraints from the Andaman Sea and Sagaing Fault constrain the motion of the West Burma Block back to 28 Ma (see Section 2.1). We subsequently connected the West Burma Block in latitude to with the Australian Plate from ~28 Ma back in time, which when placed in the paleomagnetic reference frame of Torsvik et al. (2012) results in a stable paleolatitude from the Eocene back to Cretaceous time, as predicted by Westerweel et al. (2019)'s paleomagnetic data, and an eastward motion of West Burma relative to Sundaland and the Andaman ophiolites that we reconstruct in the Sunda forearc (see Section 2.1), but at a latitude of ~2-3°S. This well within the spread in paleomagnetic poles from which Torsvik et al. (2012)'s APWP was calculated (see Rowley, 2019), and avoids inferring a Cretaceous to Eocene spreading ridge between Australia and West Burma. The Eocene clockwise rotation of the West Burma Block inferred by Westerweel et al. (2019), and also displayed in our reconstruction, is readily explained by interaction of the modern northern part of the west Burma Block with the passing Indian continent while the modern southern part still moves together with Australia, placing the scenario of Westerweel et al. (2019) straightforwardly in plate kinematic context. Nonetheless, using the somewhat more southerly latitude of Westerweel et al. (2019) would permit the same the provenance history of the Andaman Islands as interpreted below, which is the main point of our paper.

The West Burma Block, which itself was above a subduction zone in the Cretaceous, maintained a stable, near-equatorial paleolatitude from ~95–40 Ma (Westerweel et al., 2019; Fig. 13A). Placing tectonic reconstructions of SE Asia relative to Eurasia (Advokaat et al., 2018b; Hall, 2002; Li et al., 2017) in a paleomagnetic frame of reference (Torsvik et al., 2012) reveals that Sumatra, and by inference the Andaman and Nicobar forearc, was at a similar paleolatitude. This suggests that the West Burma Block must have been located to the west of, and in an intra-oceanic position within the Neotethys, in this time interval, as already proposed by Westerweel et al. (2019). The uplift and deposition of West Burma-derived sediments on the Andaman ophiolites then likely reflect the underthrusting of the eastern margin of the West Burma Block below the Andaman forearc, far enough to uplift the Andaman ophiolites, but keeping the Andaman forearc submerged to remain in a basin floor position (Fig. 13A). This requires that the West Burma Block was moving eastwards towards Sundaland, while remaining at the same paleolatitude. Westerweel et al. (2019) concluded from the stationary paleolatitude of the West Burma Block that it must have been located above a subduction zone consuming Indian plate lithosphere that at that time was rapidly moving northward, and we subscribe to that conclusion. However, to explain the simultaneous eastward motion of West Burma, we offer an alternative scenario to Westerweel et al. (2019): We note that the Australian plate, that moved northward relative to Eurasia after ~50 Ma in tandem with India, moved eastward before that time, since ~130 Ma (Torsvik et al., 2012), see also Advokaat et al. (2018a). Motion of the West Burma Block as part of the Australian plate would explain the Cretaceous-Miocene paleolatitudinal constraints of West Burma of (Westerweel et al., 2019; 2020), while at the same time explaining

E-W convergence in the Cretaceous to Eocene. In this scenario, the subduction zone below the West Burma Block may have formed a left-stepping segment on an overall N-S trending transform-dominated India-Australia plate boundary (Fig. 13A), and would not necessitate a connection to an equatorial intra-oceanic subduction zones that may (Jagoutz et al., 2015; Martin et al., 2020; Parsons et al., 2020) or may not (Borneman et al., 2015; Garzanti and Hu, 2015; van Hinsbergen et al., 2019) have existed farther to the west within the Neotethys Ocean.

The deposition of the Namunagarh Grit occurred within the time interval in which eastward Australian motion changed to northward, and in which the West Burma Block starts its northward paleolatitudinal flight at a rate similar to the Indo-Australian Plate (Westerweel et al., 2019; 2020, Fig. 13B). Constraints from the Andaman Sea and the northern Sagaing Fault suggest that by mid-Oligocene time, the West Burma Block was in a position north of the Woyla Arc, along the west Sundaland margin (Curray, 2005; Morley and Arboit, 2019). We thus infer that the West Burma Block moved northward along the Andaman forearc during the early–late Eocene, moved eastwards during the early Oligocene, and was juxtaposed against the Mogok Belt of western Sundaland by late Oligocene time (see also Westerweel et al., 2019, Fig. 13B, C). This northward motion of the West Burma Block occurred at a rate consistent with Indo-Australia – Eurasia motion, which was oblique to the Sundaland margin, and requires ongoing subduction below West Burma in this time interval. This northward motion explains why the West-Burma Block had become a more distal sediment source by the time the East Andaman Flysch started to be deposited (Fig. 13C). From the late Oligocene onward, northward motion of the West Burma Block became accommodated along the Sagaing Fault, and by extension in the Andaman Sea, and the Andaman Ophiolites became separated from the northwest Sumatra margin. The associated extension is a likely candidate to explain the major subsidence that the Andaman Ophiolites experienced before the deposition of the East Andaman Flysch. This separation juxtaposed the Andaman Ophiolites against the NNW-SSE opening Andaman Sea Basin, which provided a pathway for sediments from the continental margin of western Sundaland to reach the Andaman Ophiolites. Finally, sediments of the West Andaman Flysch, derived at least in part from the Himalaya and Indian margin, were in or after the early Miocene, but before the middle-upper Miocene cover of the Archipelago Group, accreted to the Andaman Ophiolites, showing that the Andaman Islands were by that time facing Indian oceanic lithosphere, and that the Bengal-Nicobar fan had reached the Andaman segment of the Sunda trench (Fig. 13C).

Finally, in middle to late Miocene time, the Andaman forearc started shortening again as expressed by thrusts that cut sequences as young as the Archipelago Group, and the Andaman and Nicobar Ridge started to uplift (Fig. 13D). The cause of uplift is enigmatic. Perhaps seamounts of the Ninetyeast Ridge underthrusted the forearc, or perhaps underplating of the Nicobar fan caused uplift. Regardless of the causes, the final uplift led to isolation of the islands and dominantly locally derived clastics and open marine carbonate sedimentation started to dominate the depositional process, while the Andaman Sea deepened and eventually became oceanic.

The Cenozoic northward flight of the West Burma Block suggested by recent paleomagnetic data (Westerweel et al., 2019; 2020) still contains many enigmatic predictions that will require future in-depth analysis of the geology of Myanmar. The predicted late Oligocene suture between the West Burma Block and the Sundaland margin may be consistent with exhumed ductile dextral shear zone exposed along the western Sundaland Margin (the Shan Scarp: Bertrand et al., 1999; 2001). Moreover, along the Sagaing Fault, there are relics of Lower Cretaceous radiolarian chert (Suzuki et al., 2020) and amphibolites with preliminary ages similar to the Andaman Ophiolites (Lai et al., 2018). Before Westerweel et al. (2019), these records have not been interpreted as a young suture zone. The Andaman Sea must host the original contact between the West Burma Block and the Woyla Arc (Morley et al., 2021), but whether this contact is as young as early Oligocene had not been previously estimated from the geological record. These, and many other predictions of the high Cenozoic mobility of the West Burma Block, as well as the major clockwise rotations that have been paleomagnetically documented from the block in both Cretaceous, but also post-Eocene time (Li et al., 2020; Westerweel et al., 2019; 2020), will undoubtedly be the subject of future study and debate. In our contribution, however, we note that this scenario of high mobility provides ample opportunity to explain the hitherto highly enigmatic stratigraphic-sedimentological evolution of the Andaman-Nicobar forearc, and the strong vertical motions that it experienced, which overall fit well with the first paleolatitudinal constraints that have recently been published from the West Burma Block (Westerweel et al., 2019; 2020).

6. Conclusions

The ophiolites of the Andaman Islands, located in the forearc of the Sunda subduction zone between Sumatra and Myanmar in the eastern Indian Ocean, contain a surprisingly variable stratigraphy consisting of deepwater Cretaceous and middle Eocene (hemi-)pelagic cherts and mudstones, Paleocene-lower Eocene shallow-water arc-derived clastic sediments, Oligocene-lower Miocene deep-marine turbiditic sequences, and middle Miocene and younger shallow-water limestones. These reveal rapid changes in vertical motions as well as major changes in sediment provenance whose origin have hitherto remained enigmatic. In this paper, we study the provenance of the clastic sedimentary formations, through sediment petrography, geochemistry, and U–Pb detrital zircon age spectra, and evaluate their formation and depositional environment in context of recent paleomagnetic findings that suggest that the West Burma Block occupied an equatorial paleolatitude from the Late Cretaceous to Eocene, much farther south than previously assumed, and at a similar latitude as the Andaman Ophiolites in the Sumatra forearc. Our conclusions are summarized as follows:

(1) After a Late Cretaceous period of (hemi-)pelagic, deepwater sedimentation, the Andaman Ophiolites were uplifted to shallow-water conditions, and the Namunagarh Grit was deposited comprising sediments derived from a proximal sediment source that hosted an active volcanic arc. Detrital zircon data show a ~60 Ma age for this arc. Combined with abundant 70–80 Ma zircons from Central Myanmar basin, but the absence of a preserved 80–60 Ma arc in the West Burma Block or on the Sundaland margin, we tentatively suggest that the Cretaceous Wuntho-Popa arc of the West Burma Block migrated away from the trench into the ocean in the hinterland of the West Burma Block in this time period. When this arc arrived in the Andaman trench, it likely became the dominant source of the Namunagarh Grit.
(2) Following a middle Eocene period of rapid subsidence and sediment starvation reflected in renewed chert deposition, clastic sedimentation in Oligocene to early Miocene time deposited the East Andaman Flysch on the ophiolites and overlying sediments. The East Andaman Flysch represents a distal turbiditic system derived not only from the West Burma Block, but also from a more distal continental margin source that likely was the west Sundaland margin, to the east of the Andaman Sea.

(3) The lower Miocene West Andaman Flysch, west of the Jarawa Fault, as well as the Great Nicobar Flysch also contain sediments derived from the India-Asia collision zone and likely represent an accretionary prism derived from the Nicobar Fan that was scraped off from the subducted Indian plate.
(4) We interpret the Paleocene–early Eocene uplift and shallow-marine coarse clastic sediment deposition on the Andaman Ophiolites a signature of the collision of the West Burma Block and its associated arc with the Sunda trench. This collision, following a prolonged period of E-W convergence, fits well with published paleolatitudes if we assume that the West Burma Block moved as part of the Australian Plate.
(5) We interpret renewed subsidence of the Andaman forearc and sediment starvation as the result of the northward motion of the West Burma Block after the middle Eocene, together with Australia. The East Andaman Flysch was deposited when the initial opening of the Andaman Sea opened a pathway for sediments from the western Sundaland margin to reach the Andaman forearc.
(6) While we acknowledge that the recent paleomagnetism-based scenario for the West Burma Block leaves plenty of questions open for the geology of Myanmar, and requires reinterpretation of existing datasets, we note that this newly realized mobility opens a straightforward avenue towards explaining the hitherto enigmatic sedimentary evolution of the Andaman and Nicobar Islands.

CRediT authorship contribution statement

Conceptualization: PCB, DJJvH, AL, ELA Data curation: PCB, DP, AL, AD Formal analysis: PCB, DP, AL Funding Acquisition: DJJvH Investigation: All authors Writing – original draft: PCB, DJJvH, AL, ELA Writing – review and editing: all authors.

Declaration of Competing Interest

The authors declare that they have no known competing financial interests or personal relationships that could have appeared to influence the work reported in this paper.

Acknowledgements

DJJvH acknowledges NWO Vici grant 865.17.001. We thank Yael Engbers for help in the field. Anita van Leeuwen-Tolboom is thanked for help in the lab. We acknowledge Sarah Kachovich for additional micropaleontological and petrological observations that confirmed the age of the middle Eocene radiolarian chert and siliceous mudstone from Chidiya Tapu. We thank Chris Morley, Andrew Carter, and associate editor Ian Somerville for their constructive comments that helped to improve this paper.

Appendix A. Supplementary material

Supplementary data to this article can be found online at https://doi.org/10.1016/j.gr.2021.10.011.

References

Advokaat, E.L., Bongers, M.L.M., Rudyawan, A., BouDagher-Fadel, M.K., Langereis, C. G., van Hinsbergen, D.J.J., 2018a. Early Cretaceous origin of the Woyla Arc (Sumatra, Indonesia) on the Australian plate. Earth Planet. Sci. Lett. 498, 348–361.
Advokaat, E.L., Marshall, N.T., Li, S., Spakman, W., Krijgsman, W., van Hinsbergen, D. J.J., 2018b. Cenozoic rotation history of Borneo and Sundaland, SE Asia revealed by paleomagnetism, seismic tomography, and kinematic reconstruction. Tectonics 37 (8), 2486–2512.
Ahmedali, S.T., 1989. X-ray fluorescence analysis in the geological sciences: Advances in methodology. St. John's, Nfld.: Geological Association of Canada= Association géologique . . ..
Aitchison, J.C., Ali, J.R., Davis, A.M., 2007. When and where did India and Asia collide? J. Geophys. Res. 112 (B5). https://doi.org/10.1029/2006JB004706.
Aitchison, J.C., Ao, A., Bhowmik, S., Clarke, G.L., Ireland, T.R., Kachovich, S., Lokho, K., Stojanovic, D., Roeder, T., Truscott, N., Zhen, Y., Zhou, R., 2019. Tectonic evolution of the western margin of the Burma microplate based on new fossil and radiometric age constraints. Tectonics 38 (5), 1718–1741.
Allen, R., Carter, A., Najman, Y., Bandopadhyay, P., Chapman, H., Bickle, M., Garzanti, E., Vezzoli, G., Andò, S., Foster, G., 2008. New constraints on the sedimentation and uplift history of the Andaman-Nicobar accretionary prism, South Andaman Island. Geol. Soc. Am. Spec. Pap. 436, 223.
Arboit, F., Min, M., Chew, D., Mitchell, A., Drost, K., Badenszki, E., Daly, J.S., 2021. Constraining the links between the Himalayan belt and the Central Myanmar basins during the Cenozoic: an integrated multi-proxy detrital geochronology and trace-element geochemistry study. Geosci. Front. 12 (2), 657–676.
Armstrong-Altrin, J.S., Lee, Y.I., Kasper-Zubillaga, J.J., Carranza-Edwards, A., Garcia, D., Eby, G.N., Balaram, V., Cruz-Ortiz, N.L., 2012. Geochemistry of beach sands along the western Gulf of Mexico, Mexico: implication for provenance. Geochemistry 72 (4), 345–362.
Armstrong-Altrin, J.S., Nagarajan, R., Madhavaraju, J., Rosalez-Hoz, L., Lee, Y.I., Balaram, V., Cruz-Martínez, A., Avila-Ramírez, G., 2013. Geochemistry of the Jurassic and Upper Cretaceous shales from the Molango Region, Hidalgo, eastern Mexico: Implications for source-area weathering, provenance, and tectonic setting. C.R. Geosci. 345 (4), 185–202.
Awasthi, N., 2017. Provenance and paleo–weathering of Tertiary accretionary prism–forearc sedimentary deposits of the Andaman Archipelago, India. J. Asian Earth Sci. 150, 45–62.
Awasthi, N., Ray, J.S., 2020. The Palaeogene record of Himalayan erosion in the Andaman Basin. J. Earth Syst. Sci. 129, 1–16.
Bandopadhyay, P., Carter, A., 2017a. Mithakhari deposits. Geol. Soc., London, Memoirs 47, 111–132.
Bandopadhyay, P., Carter, A., 2017b. Submarine fan deposits: petrography and geochemistry of the Andaman Flysch. Geol. Soc., London, Memoirs 47, 133–140.
Bandopadhyay, P., Carter, A., 2017c. The archipelago group: current understanding. Geol. Soc., London, Memoirs 47, 153–166.
Bandopadhyay, P.C., Chakrabarti, U., Roy, A., 2009. First report of trace fossils from Palaeogene succession (Namunagarh Grit) of Andaman and Nicobar Islands. J. Geol. Soc. India 73 (2), 261–267.
Bandopadhyay, P., Ghosh, B., 1998. Facies, petrology and depositional environment of the Tertiary sedimentary rocks, around Port Blair, South Andaman. J. Geol. Soc. India 52, 53–66.
Bandopadhyay, P.C., Ghosh, Biswajit, 2015. Provenance analysis of the Oligocene turbidites (Andaman Flysch), South Andaman Island: a geochemical approach. J. Earth Syst. Sci. 124 (5), 1019–1037.
Bandopadhyay, P.C., 2005. Discovery of abundant pyroclasts in the Namunagarh Grit, South Andaman: evidence for arc volcanism and active subduction during the Palaeogene in the Andaman area. J. Asian Earth Sci. 25 (1), 95–107.
Bandopadhyay, P.C., 2012. Re-interpretation of the age and environment of deposition of Paleogene turbidites in the Andaman and Nicobar Islands, Western Sunda Arc. J. Asian Earth Sci. 45, 126–137.
Bandyopadhyay, D., Ghosh, B., Guilmette, C., Plunder, A., Corfu, F., Advokaat, E.L., Bandopadhyay, P.C., van Hinsbergen, D.J.J., 2021. Geochemical and geochronological record of the Andaman Ophiolite, SE Asia: From back-arc to forearc during subduction polarity reversal? Lithos 380-381, 105853. https://doi.org/10.1016/j.lithos.2020.105853.
Bandyopadhyay, D., van Hinsbergen, D.J.J., Plunder, A., Bandopadhyay, P.C., Advokaat, E., Chattopadhaya, S., Morishita, T., Ghosh, B., 2020. Andaman Ophiolite: An Overview. In: Ray, J.S., Radhakrishna, M. (Eds.), The Andaman Islands and Adjoining Offshore: Geology, Tectonics and Palaeoclimate. Springer International Publishing, Cham, pp. 1–17.
Barber, A.J., 2000. The origin of the Woyla Terranes in Sumatra and the Late Mesozoic evolution of the Sundaland margin. J. Asian Earth Sci. 18 (6), 713–738.
Barber, A.J., Crow, M.J., 2009. Structure of Sumatra and its implications for the tectonic assembly of Southeast Asia and the destruction of Paleotethys. Island Arc 18, 3-20.
Barber, A.J., Crow, M.J., De Smet, M.E.M., 2005. Chapter 14 Tectonic Evolution. Geological Society, London, Memoirs 31, 234-259.
Basu, A., 1985. Reading provenance from detrital quartz, Provenance of arenites. Springer, pp. 231-247.
Baxter, A.T., Aitchison, J.C., Zyabrev, S.V., Ali, J.R., 2011. Upper Jurassic radiolarians from the Naga ophiolite, Nagaland, northeast India. Gondwana Res. 20 (2-3), 638–644.
Bertrand, G., Rangin, C., 2003. Tectonics of the western margin of the Shan plateau (central Myanmar): implication for the India-Indochina oblique convergence since the Oligocene. J. Asian Earth Sci. 21 (10), 1139–1157.
Bertrand, G., Rangin, C., Maluski, H., Bellon, H., Party, G.S., 2001. Diachronous cooling along the Mogok Metamorphic Belt (Shan scarp, Myanmar): the trace of the northward migration of the Indian syntaxis. J. Asian Earth Sci. 19, 649–659.
Bertrand, G., Rangin, C., Maluski, H., Han, T.A., Thein, M., Myint, O., Maw, W., Lwin, S., 1999. Cenozoic metamorphism along the Shan scarp (Myanmar): evidences for ductile shear along the Sagaing fault or the northward migration of the eastern Himalayan syntaxis? Geophys. Res. Lett. 26 (7), 915–918.

Bhat, M.I., Ghosh, S.K., 2001. Geochemistry of the 2.51 Ga old Rampur group pelites, western Himalayas: implications for their provenance and weathering. Precambr. Res. 108 (1-2), 1–16.
Bhatia, M.R., Crook, K.A.W., 1986. Trace element characteristics of graywackes and tectonic setting discrimination of sedimentary basins. Contrib. Miner. Petrol. 92 (2), 181–193.
Borneman, N.L., Hodges, K.V., van Soest, M.C., Bohon, W., Wartho, J.-A., Cronk, S.S., Ahmad, T., 2015. Age and structure of the Shyok suture in the Ladakh region of northwestern India: implications for slip on the Karakoram fault system. Tectonics 34 (10), 2011–2033.
Bracciali, L., Najman, Y., Parrish, R.R., Akhter, S.H., Millar, I., 2015. The Brahmaputra tale of tectonics and erosion: Early Miocene river capture in the Eastern Himalaya. Earth Planet. Sci. Lett. 415, 25–37.
Cai, F., Ding, L., Zhang, Q., Orme, D.A., Wei, H., Li, J., Zhang, J.e., Zaw, T., Sein, K., 2020. Initiation and evolution of forearc basins in the Central Myanmar Depression. Geol. Soc. Am. Bull. 132, 1066-1082.
Chakraborty, P., 1999. Facies pattern and depositional motif in an immature trench-slope basin, Eocene Mithakhari Group, Middle Andaman, India. J. Geol. Soc. India 53, 271–284.
Chakraborty, P.P., Pal, T., 2001. Anatomy of a forearc submarine fan: Upper Eocene—Oligocene Andaman Flysch Group, Andaman Islands, India. Gondwana Res. 4 (3), 477–486.
Chatterjee, A., 1964. The tertiary fauna of Andaman, International Geological Congress Report, 22nd Session, New Delhi, p. 318.
Chen, W.-H., Yan, Y.i., Clift, P.D., Carter, A., Huang, C.-Y., Pickering, K.T., Chemale, F., Shan, Y., Zhang, X., 2020. Drainage evolution and exhumation history of the eastern Himalaya: Insights from the Nicobar Fan, northeastern Indian Ocean. Earth Planet. Sci. Lett. 548, 116472. https://doi.org/10.1016/j.epsl.2020.116472.
Clift, P.D., Hodges, K.V., Heslop, D., Hannigan, R., Van Long, H., Calves, G., 2008. Correlation of Himalayan exhumation rates and Asian monsoon intensity. Nat. Geosci. 1 (12), 875–880.
Condie, K.C., 1993. Chemical composition and evolution of the upper continental crust: contrasting results from surface samples and shales. Chem. Geol. 104 (1-4), 1–37.
Cox, R., Lowe, D.R., Cullers, R.L., 1995. The influence of sediment recycling and basement composition on evolution of mudrock chemistry in the southwestern United States. Geochim. Cosmochim. Acta 59 (14), 2919–2940.
Critelli, S., Le Pera, E., 1994. Detrital modes and provenance of Miocene sandstones and modern sands to the Southern Apennines thrust-top basins (Italy). Journal of Sedimentary Research 64 (4a), 824–835.
Crook, K.A., 1974. Lithogenesis and geotectonics: the significance of compositional variation in flysch arenites (graywackes).
Cullers, R.L., Basu, A., Suttner, L.J., 1988. Geochemical signature of provenance in sand-size material in soils and stream sediments near the Tobacco Root batholith, Montana, USA. Chem. Geol. 70 (4), 335–348.
Cullers, R.L., Podkovyrov, V.N., 2000. Geochemistry of the Mesoproterozoic Lakhanda shales in southeastern Yakutia, Russia: implications for mineralogical and provenance control, and recycling. Precambr. Res. 104, 77–93.
Curray, J., Allen, R., 2008. Evolution, paleogeography and sediment provenance, Bay of Bengal, Indian Ocean. Recent Advances in Earth System Sciences (Golden Jubilee Volume). Geol Soc India Mem 66, 487–520.
Curray, J., Moore, D., Lawver, L., Emmel, F., Raitt, R., Henry, M., Kieckhefer, R., 1979. Tectonics of the Andaman Sea and Burma: convergent margins.
Curray, J.R., 2005. Tectonics and history of the Andaman Sea region. J. Asian Earth Sci. 25 (1), 187–232.
Dickinson, W.R., 1970. Interpreting detrital modes of graywacke and arkose. J. Sediment. Res. 40, 695–707.
Dickinson, W.R., 1985. Interpreting provenance relations from detrital modes of sandstones, Provenance of arenites. Springer, pp. 333-361.
Dickinson, W.R., Gehrels, G.E., 2009. Use of U-Pb ages of detrital zircons to infer maximum depositional ages of strata: a test against a Colorado Plateau Mesozoic database. Earth Planet. Sci. Lett. 288 (1-2), 115–125.
Etemad-Saeed, N., Hosseini-Barzi, M., Armstrong-Altrin, J.S., 2011. Petrography and geochemistry of clastic sedimentary rocks as evidences for provenance of the Lower Cambrian Lalun Formation, Posht-e-badam block, Central Iran. J. Afr. Earth Sci. 61 (2), 142–159.
Fedo, C.M., Wayne Nesbitt, H., Young, G.M., 1995. Unraveling the effects of potassium metasomatism in sedimentary rocks and paleosols, with implications for paleoweathering conditions and provenance. Geology 23 (10), 921. https://doi.org/10.1130/0091-7613(1995)023<0921:UTEOPM>2.3.CO;2.
Fisher, R.V., Schmincke, H.-U., 1984. Submarine volcaniclastic rocks, Pyroclastic Rocks. Springer, pp. 265-296.
Frey, M., 1987. Very low-grade metamorphism of clastic sedimentary rocks. Low Temp. Metamorphism, 9–58.
Garzanti, E., Resentini, A., 2016. Provenance control on chemical indices of weathering (Taiwan river sands). Sediment. Geol. 336, 81–95.
Garzanti, E., Hu, X., 2015. Latest Cretaceous Himalayan tectonics: Obduction, collision or Deccan-related uplift? Gondwana Res. 28 (1), 165–178.
Garzanti, E., Vezzoli, G., 2003. A classification of metamorphic grains in sands based on their composition and grade. J. Sediment. Res. 73 (5), 830–837.
Ghosh, B., Pal, T., Bhattacharya, A., Das, D., 2009. Petrogenetic implications of ophiolitic chromite from Rutland Island, Andaman—a boninitic parentage in supra-subduction setting. Mineral. Petrol. 96 (1-2), 59–70.
Girty, G.H., Hanson, A.D., Knaack, C., Johnson, D., 1994. Provenance determined by REE, Th, and Sc analyses of metasedimentary rocks, Boyden Cave roof pendant, central Sierra Nevada, California. J. Sediment. Res. 64, 68–73.
Hall, R., 2002. Cenozoic geological and plate tectonic evolution of SE Asia and the SW Pacific: computer-based reconstructions, model and animations. J. Asian Earth Sci. 20 (4), 353–431.
Hall, R., 2012. Late Jurassic-Cenozoic reconstructions of the Indonesian region and the Indian Ocean. Tectonophysics 570-571, 1–41.
Hamilton, W.B., 1988. Plate tectonics and island arcs. Geol. Soc. Am. Bull. 100, 1503–1527.
Hayashi, K.-I., Fujisawa, H., Holland, H.D., Ohmoto, H., 1997. Geochemistry of~ 1.9 Ga sedimentary rocks from northeastern Labrador, Canada. Geochim. Cosmochim. Acta 61 (19), 4115–4137.
Herron, M.M., 1988. Geochemical classification of terrigenous sands and shales from core or log data. J. Sediment. Res. 58, 820–829.
Horstwood, M.S., Košler, J., Gehrels, G., Jackson, S.E., McLean, N.M., Paton, C., Pearson, N.J., Sircombe, K., Sylvester, P., Vermeesch, P., 2016. Community-derived standards for LA-ICP-MS U-(Th-) Pb geochronology–Uncertainty propagation, age interpretation and data reporting. Geostand. Geoanal. Res. 40, 311–332.
Hu, X., Garzanti, E., Wang, J., Huang, W., An, W., Webb, A., 2016. The timing of India-Asia collision onset – Facts, theories, controversies. Earth Sci. Rev. 160, 264–299.
Huchon, P., Le Pichon, X., 1984. Sunda Strait and central Sumatra fault. Geology 12 (11), 668. https://doi.org/10.1130/0091-7613(1984)12<668:SSACSF>2.0.CO;2.
Jafri, S.H., Balaram, V., Govil, P.K., 1993. Depositional environments of Cretaceous radiolarian cherts from Andaman-Nicobar islands, northeastern Indian Ocean. Mar. Geol. 112 (1-4), 291–301.
Jagoutz, O., Royden, L., Holt, A.F., Becker, T.W., 2015. Anomalously fast convergence of India and Eurasia caused by double subduction. Nat. Geosci. 8 (6), 475–478.
Jenner, G.A., Longerich, H.P., Jackson, S.E., Fryer, B.J., 1990. ICP-MS—A powerful tool for high-precision trace-element analysis in Earth sciences: Evidence from analysis of selected USGS reference samples. Chem. Geol. 83 (1-2), 133–148.
Joo, Y.J., Lee, Y.I., Bai, Z., 2005. Provenance of the Qingshuijian Formation (Late Carboniferous), NE China: Implications for tectonic processes in the northern margin of the North China block. Sed. Geol. 177 (1-2), 97–114.
Kapp, P., DeCelles, P.G., 2019. Mesozoic-Cenozoic geological evolution of the Himalayan-Tibetan orogen and working tectonic hypotheses. Am. J. Sci. 319 (3), 159–254.
Karunakaran, C., 1968. Tertiary sedimentation in the Andaman-Nicobar geosyncline. J. Geol. Soc. India 9, 32–39.
Kübler, B., 1968. Evaluation quantitative du métamorphisme par la cristallinité de l'illite. Bulletin Centre de Researches de Pau-SNPA 2, 385–397.
Lai, C.-K., Zaw, K., Meffre, S., 2018. Multiphase magmatism of the Neotethyan Central Ophiolite Belt in Myanmar: Zircon U-Pb age and whole-rock geochemical constraints from the Sagaing-Minwun ophiolite. EGUGA, 3587.
Lamont, T.N., Searle, M.P., Hacker, B.R., Htun, K., Htun, K.M., Morley, C.K., Waters, D. J., White, R.W., 2021. Late Eocene-Oligocene granulite facies garnet-sillimanite migmatites from the Mogok Metamorphic belt, Myanmar, and implications for timing of slip along the Sagaing Fault. Lithos 386-387, 106027. https://doi.org/10.1016/j.lithos.2021.106027.
Le Maitre, R., Streckeisen, A., Zanettin, B., Le Bas, M., Bonin, B., Bateman, P., Bellieni, G., Dudek, A., Efremova, S., Keller, J., 2002. Igneous rocks. A classification and glossary of terms 2.
Lechler, P.J., Desilets, M.O., 1987. A review of the use of loss on ignition as a measurement of total volatiles in whole-rock analysis. Chem. Geol. 63 (3-4), 341–344.
Lee, Y.I., 2009. Geochemistry of shales of the Upper Cretaceous Hayang Group, SE Korea: Implications for provenance and source weathering at an active continental margin. Sed. Geol. 215 (1-4), 1–12.
Lelgemann, H., Gutscher, M.-A., Bialas, J., Flueh, E.R., Weinrebe, W., Reichert, C., 2000. Transtensional basins in the western Sunda Strait. Geophys. Res. Lett. 27 (21), 3545–3548.
Li, J.-X., Fan, W.-M., Zhang, L.-Y., Evans, N.J., Sun, Y.-L., Ding, L., Guan, Q.-Y., Peng, T.-P., Cai, F.-L., Sein, K., 2019. Geochronology, geochemistry and Sr–Nd–Hf isotopic compositions of Late Cretaceous-Eocene granites in southern Myanmar: Petrogenetic, tectonic and metallogenic implications. Ore Geol. Rev. 112, 103031. https://doi.org/10.1016/j.oregeorev.2019.103031.
Li, S., Advokaat, E.L., van Hinsbergen, D.J.J., Koymans, M., Deng, C., Zhu, R., 2017. Paleomagnetic constraints on the Mesozoic-Cenozoic paleolatitudinal and rotational history of Indochina and South China: Review and updated kinematic reconstruction. Earth Sci. Rev. 171, 58–77.
Li, Z., Ding, L., Zaw, T., Wang, H., Cai, F., Yao, W., Xiong, Z., Sein, K., Yue, Y., 2020. Kinematic evolution of the West Burma block during and after India-Asia collision revealed by paleomagnetism. J. Geodyn. 134, 101690. https://doi.org/10.1016/j.jog.2019.101690.
Licht, A., Dupont-Nivet, G., Win, Z., Swe, H.H., Kaythi, M., Roperch, P., Ugrai, T., Littell, V., Park, D., Westerweel, J., 2019. Paleogene evolution of the Burmese forearc basin and implications for the history of India-Asia convergence. GSA Bull. 131, 730–748.
Licht, A., Win, Z., Westerweel, J., Cogné, N., Morley, C.K., Chantraprasert, S., Poblete, F., Ugrai, T., Nelson, B., Aung, D.W., Dupont-Nivet, G., 2020. Magmatic history of central Myanmar and implications for the evolution of the Burma Terrane. Gondwana Res. 87, 303–319.
Limonta, M., Resentini, A., Carter, A., Bandopadhyay, P.C., Garzanti, E., 2017. Provenance of Oligocene Andaman sandstones (Andaman–Nicobar Islands):

Ganga-Brahmaputra or Irrawaddy derived? Geol. Soc., London, Memoirs 47, 141–152.
Ling, H.Y., Chandra, R., Karkare, S.G., 1996. Tectonic significance of eocene and cretaceous radiolaria from south andaman island, northeast indian ocean. Isl. Arc 5 (2), 166–179.
Ling, H.Y., Srinivasan, M., 1993. Significance of Eocene radiolaria from port Blair group of south Andaman island, India. J. Paheontol. Soc. India 38, 1–5.
Liu, C.-Z., Chung, S.-L., Wu, F.-Y., Zhang, C., Xu, Y., Wang, J.-G., Chen, Y.i., Guo, S., 2016. Tethyan suturing in Southeast Asia: Zircon U-Pb and Hf-O isotopic constraints from Myanmar ophiolites. Geology 44 (4), 311–314.
Long, X., Sun, M., Yuan, C., Xiao, W., Cai, K., 2008. Early Paleozoic sedimentary record of the Chinese Altai: implications for its tectonic evolution. Sed. Geol. 208 (3-4), 88–100.
Longerich, H.P., 1995. Analysis of pressed pellets of geological samples using wavelength-dispersive x-ray fluorescence spectrometry. X-Ray Spectrom. 24 (3), 123–136.
Ludwig, K.R., 2003. Isoplot 3.00: A geochronological toolkit for Microsoft Excel. Berkeley Geochronol. Center Spec. Publ. 4, 70.
Madhavaraju, J., 2015. Geochemistry of late cretaceous sedimentary rocks of the Cauvery Basin, South India: constraints on paleoweathering, provenance, and end cretaceous environments, Chemostratigraphy. Elsevier, pp. 185-214.
Martin, C.R., Jagoutz, O., Upadhyay, R., Royden, L.H., Eddy, M.P., Bailey, E., Nichols, C.I.O., Weiss, B.P., 2020. Paleocene latitude of the Kohistan-Ladakh arc indicates multistage India-Eurasia collision. Proc. Natl. Acad. Sci. 117 (47), 29487–29494.
McLennan, S., Hemming, S., McDaniel, D., Hanson, G., 1993. Geochemical approaches to sedimentation, provenance, and tectonics. Spec. Papers-Geol. Soc. Am.
McLennan, S.M., Taylor, S.R., McCulloch, M.T., Maynard, J.B., 1990. Geochemical and Nd Sr isotopic composition of deep-sea turbidites: crustal evolution and plate tectonic associations. Geochim. Cosmochim. Acta 54 (7), 2015–2050.
McLennan, S.M., 1989. Rare earth elements in sedimentary rocks: influence of provenance and sedimentary processes. Geochem. Mineral. Rare Earth Elements, Rev. Mineral. 21, 169–200.
McNeill, L.C., Dugan, B., Backman, J., Pickering, K.T., Pouderoux, H.F.A., Henstock, T.J., Petronotis, K.E., Carter, A., Chemale, F., Milliken, K.L., Kutterolf, S., Mukoyoshi, H., Chen, W., Kachovich, S., Mitchison, F.L., Bourlange, S., Colson, T.A., Frederik, M.C.G., Guèrin, G., Hamahashi, M., House, B.M., Hüpers, A., Jeppson, T.N., Kenigsberg, A.R., Kuranaga, M., Nair, N., Owari, S., Shan, Y., Song, I., Torres, M.E., Vannucchi, P., Vrolijk, P.J., Yang, T., Zhao, X., Thomas, E., 2017. Understanding Himalayan erosion and the significance of the Nicobar Fan. Earth Planet. Sci. Lett. 475, 134–142.
Metcalfe, I., 2013. Gondwana dispersion and Asian accretion: Tectonic and palaeogeographic evolution of eastern Tethys. J. Asian Earth Sci. 66, 1–33.
Morley, C., 2017. Cenozoic rifting, passive margin development and strike-slip faulting in the Andaman Sea: a discussion of established v. new tectonic models. Geol. Soc., London, Memoirs 47, 27–50.
Morley, C.K., Alvey, A., 2015. Is spreading prolonged, episodic or incipient in the Andaman Sea? Evidence from deepwater sedimentation. J. Asian Earth Sci. 98, 446–456.
Morley, C., Arboit, F., 2019. Dating the onset of motion on the Sagaing fault: Evidence from detrital zircon and titanite U-Pb geochronology from the North Minwun Basin, Myanmar. Geology 47, 581-585.
Morley, C., Chantraprasert, S., Kongchum, J., Chenoll, K., 2021. The West Burma Terrane, a review of recent paleo-latitude data, its geological implications and constraints. Earth-Science Reviews 103722.
Morley, C.K., Tin Tin Naing, Searle, M., Robinson, S.A., 2020. Structural and tectonic development of the Indo-Burma ranges. Earth-Science Rev. 200, 102992. https://doi.org/10.1016/j.earscirev.2019.102992.
Morley, C.K., Searle, M., 2017. Regional tectonics, structure and evolution of the Andaman-Nicobar Islands from ophiolite formation and obduction to collision and back-arc spreading. Geol. Soc. London, Mem. 47, 51–74.
Morton, A.C., Hallsworth, C., 1994. Identifying provenance-specific features of detrital heavy mineral assemblages in sandstones. Sed. Geol. 90 (3-4), 241–256.
Mukhopadhyay, B., Chakraborty, P.P., Paul, S., 2003. Facies clustering in turbidite successions: case study from Andaman Flysch Group, Andaman Islands, India. Gondwana Res. 6, 918–925.
Müller, R.D., Seton, M., Zahirovic, S., Williams, S.E., Matthews, K.J., Wright, N.M., Shephard, G.E., Maloney, K.T., Barnett-Moore, N., Hosseinpour, M., Bower, D.J., Cannon, J., 2016. Ocean Basin Evolution and Global-Scale Plate Reorganization Events Since Pangea Breakup. Annu. Rev. Earth Planet. Sci. 44 (1), 107–138.
Najman, Y., Bickle, M., Garzanti, E., Pringle, M., Barfod, D., Brozovic, N., Burbank, D., Ando, S., 2009. Reconstructing the exhumation history of the Lesser Himalaya, NW India, from a multitechnique provenance study of the foreland basin Siwalik Group. Tectonics 28 (5), n/a–n/a.
Nesbitt, H.W., Young, G.M., 1982. Early Proterozoic climates and plate motions inferred from major element chemistry of lutites. Nature 299 (5885), 715–717.
Nesbitt, H.W., Young, G.M., 1984. Prediction of some weathering trends of plutonic and volcanic rocks based on thermodynamic and kinetic considerations. Geochim. Cosmochim. Acta 48 (7), 1523–1534.
Oo, K.L., Zaw, K., Meffre, S., Aung, D.W., Lai, C.-K., 2015. Provenance of the Eocene sandstones in the southern Chindwin Basin, Myanmar: Implications for the unroofing history of the Cretaceous-Eocene magmatic arc. J. Asian Earth Sci. 107, 172–194.
Pal, T., 2011. Petrology and geochemistry of the Andaman ophiolite: melt-rock interaction in a suprasubduction-zone setting. J. Geol. Soc. 168 (4), 1031–1045.
Pal, T., Bhattacharya, A., 2010. Greenschist-facies sub-ophiolitic metamorphic rocks of Andaman Islands, Burma-Java subduction complex. J. Asian Earth Sci. 39 (6), 804–814.
Pal, T., Chakraborty, P.P., Gupta, T.D., Singh, C.D., 2003. Geodynamic evolution of the outer-arcforearc belt in the Andaman Islands, the central part of the BurmaJava subduction complex. Geol. Mag. 140, 289-307.
Parker, A., 1970. An index of weathering for silicate rocks. Geol. Mag. 107 (6), 501–504.
Parsons, A.J., Hosseini, K., Palin, R.M., Sigloch, K., 2020. Geological, geophysical and plate kinematic constraints for models of the India-Asia collision and the post-Triassic central Tethys oceans. Earth Sci. Rev. 208, 103084. https://doi.org/10.1016/j.earscirev.2020.103084.
Paton, C., Woodhead, J.D., Hellstrom, J.C., Hergt, J.M., Greig, A., Maas, R., 2010. Improved laser ablation U-Pb zircon geochronology through robust downhole fractionation correction. Geochem., Geophys., Geosyst. 11.
Patriat, P., Achache, J., 1984. India-Eurasia collision chronology has implications for crustal shortening and driving mechanism of plates. Nature 311 (5987), 615–621.
Pedersen, R.B., Searle, M.P., Carter, A., Bandopadhyay, P.C., 2010. U-Pb zircon age of the Andaman ophiolite: implications for the beginning of subduction beneath the Andaman-Sumatra arc. J. Geol. Soc. 167 (6), 1105–1112.
Pettijohn, F.J., 1963. Chemical composition of sandstones, excluding carbonate and volcanic sands: Representative analyses. US Government Printing Office.
Pettijohn, F.J., Potter, P.E., Siever, R., 1972. Introduction and Source Materials, Sand and Sandstone. Springer, pp. 1-23.
Pettijohn, F.J., Potter, P.E., Siever, R., 1987. Sand and sandstone. Springer Science & Business Media.
Pickering, K.T., Pouderoux, H., McNeill, L.C., Backman, J., Chemale, F., Kutterolf, S., Milliken, K.L., Mukoyoshi, H., Henstock, T.J., Stevens, D.E., Parnell, C., Dugan, B., 2020. Sedimentology, stratigraphy and architecture of the Nicobar Fan (Bengal–Nicobar Fan System), Indian Ocean: Results from International Ocean Discovery Program Expedition 362. Sedimentology 67 (5), 2248–2281.
Pittman, E.D., 1970. Plagioclase feldspar as an indicator of provenance in sedimentary rocks. J. Sediment. Res. 40.
Plunder, A., Bandyopadhyay, D., Ganerød, M., Advokaat, E.L., Ghosh, B., Bandopadhyay, P., Hinsbergen, D.J.J., 2020. History of subduction polarity reversal during arc-continent collision: constraints from the Andaman Ophiolite and its metamorphic sole. Tectonics 39 (6). https://doi.org/10.1029/2019TC005762.
Rajkakati, M., Bhowmik, S.K., Ao, A., Ireland, T.R., Avila, J., Clarke, G.L., Bhandari, A., Aitchison, J.C., 2019. Thermal history of Early Jurassic eclogite facies metamorphism in the Nagaland Ophiolite Complex, NE India: New insights into pre-Cretaceous subduction channel tectonics within the Neo-Tethys. Lithos 346-347, 105166. https://doi.org/10.1016/j.lithos.2019.105166.
Ray, K., 1982. A review of the geology of Andaman and Nicobar islands. Miscellaneous publication-Geological survey of India, 110–125.
Roaldset, E., 1972. Mineralogy and geochemistry of Quaternary clays in the Numedal area, southern Norway.
Robinson, R.A.J., Brezina, C.A., Parrish, R.R., Horstwood, M.S.A., Nay Win, O., Bird, M. I., Myint, T., Walters, A.S., Oliver, G.J.H., Khin, Z., 2014. Large rivers and orogens: The evolution of the Yarlung Tsangpo-Irrawaddy system and the eastern Himalayan syntaxis. Gondwana Res. 26, 112–121.
Roser, B., Cooper, R., Nathan, S., Tulloch, A., 1996. Reconnaissance sandstone geochemistry, provenance, and tectonic setting of the lower Paleozoic terranes of the West Coast and Nelson, New Zealand. N. Z. J. Geol. Geophys. 39, 1–16.
Roser, B., Korsch, R., 1986. Determination of tectonic setting of sandstone-mudstone suites using SiO2 content and K2O/Na2O ratio. J. Geol. 94, 635–650.
Rowley, D.B., 2019. Comparing Paleomagnetic Study Means with Apparent Wander Paths: A Case Study and Paleomagnetic Test of the Greater India versus Greater Indian Basin Hypotheses. Tectonics 38, 722–740.
Roy, S.K., 1992. Accretionary prism in Andaman forearc. Geological Survey of India Special Publication 29, 273–278.
Rudnick, R.L., Gao, S., 2014. 4.1 - Composition of the Continental Crust. In: Holland, H.D., Turekian, K.K. (Eds.), Treatise on Geochemistry (Second Edition). Elsevier, Oxford, pp. 1–51.
Sarma, D.S., Jafri, S.H., Fletcher, I.R., McNaughton, N.J., 2010. Constraints on the Tectonic Setting of the Andaman Ophiolites, Bay of Bengal, India, from SHRIMP U-Pb Zircon Geochronology of Plagiogranite. J. Geol. 118, 691–697.
Scotese, C.R., 2004. A continental drift flipbook. J. Geol. 112, 729–741.
Seton, M., Müller, R.D., Zahirovic, S., Gaina, C., Torsvik, T., Shephard, G., Talsma, A., Gurnis, M., Turner, M., Maus, S., Chandler, M., 2012. Global continental and ocean basin reconstructions since 200Ma. Earth Sci. Rev. 113, 212–270.
Sevastjanova, I., Hall, R., Rittner, M., Paw, S.M.T.L., Naing, T.T., Alderton, D.H., Comfort, G., 2016. Myanmar and Asia united, Australia left behind long ago. Gondwana Res. 32, 24–40.
Shanmugam, G., Moiola, R., 1988. Submarine fans: characteristics, models, classification, and reservoir potential. Earth Sci. Rev. 24, 383–428.
Shepherd, T., Miller, M., Scrivener, R., Darbyshire, D., 1985. Hydrothermal fluid evolution in relation to mineralization in southwest England with special reference to the Dartmoor-Bodmin area. High Heat Production (HHP) Granites, hydrothermal circulation and ore genesis, 345-364.
Sieh, K., Natawidjaja, D., 2000. Neotectonics of the Sumatran fault, Indonesia. J. Geophys. Res. Solid Earth 105, 28295–28326.
Singh, A.K., Chung, S.-L., Bikramaditya, R.K., Lee, H.Y., 2017. New U-Pb zircon ages of plagiogranites from the Nagaland-Manipur Ophiolites, Indo-Myanmar Orogenic Belt, NE India. J. Geol. Soc. 174, 170–179.

Spears, D., 1982. The recognition of volcanic clays and the significance of heavy minerals. Clay Miner. 17, 373–375.
Stampfli, G.M., Borel, G., 2002. A plate tectonic model for the Paleozoic and Mesozoic constrained by dynamic plate boundaries and restored synthetic oceanic isochrons. Earth Planet. Sci. Lett. 196, 17–33.
Sun, S.-s., McDonough, W.F., 1989. Chemical and isotopic systematics of oceanic basalts: implications for mantle composition and processes, Geological Society, London, Special Publications, in: Saunders, A.D., Norry, M.J. (Eds.), Magmatism in the Ocean Basins 42, pp. 313-345.
Suzuki, H., Ja, L., Maung, M., Thin, A.K., Kuwahara, K., 2020. The First Report on Early Cretaceous Radiolaria from Myanmar. Paleontol. Res. 24, 103–112.
Tapponnier, P., Mattauer, M., Proust, F., Cassaigneau, C., 1981. Mesozoic ophiolites, sutures, and arge-scale tectonic movements in Afghanistan. Earth Planet. Sci. Lett. 52, 355–371.
Taylor, S.R., McLennan, S.M., 1985. The continental crust: its composition and evolution.
Than, N.M., Khin, K., Thein, M., 2017. Cretaceous geology of Myanmar and Cenozoic geology in the Central Myanmar Basin. Geol. Soc., London, Memoirs 48, 143–167.
Torsvik, T.H., Cocks, L.R.M., 2017. Earth history and palaeogeography. Cambridge University Press.
Torsvik, T.H., Van der Voo, R., Preeden, U., Mac Niocaill, C., Steinberger, B., Doubrovine, P.V., van Hinsbergen, D.J.J., Domeier, M., Gaina, C., Tohver, E., Meert, J.G., McCausland, P.J.A., Cocks, L.R.M., 2012. Phanerozoic polar wander, palaeogeography and dynamics. Earth Sci. Rev. 114, 325–368.
Tucker, M.E., 2009. Sedimentary petrology: an introduction to the origin of sedimentary rocks. John Wiley & Sons.
Vadlamani, R., Wu, F.-Y., Ji, W.-Q., 2015. Detrital zircon U-Pb age and Hf isotopic composition from foreland sediments of the Assam Basin, NE India: Constraints on sediment provenance and tectonics of the Eastern Himalaya. J. Asian Earth Sci. 111, 254–267.
van Hinsbergen, D.J.J., Kapp, P., Dupont-Nivet, G., Lippert, P.C., DeCelles, P.G., Torsvik, T.H., 2011a. Restoration of Cenozoic deformation in Asia and the size of Greater India. Tectonics 30, TC5003.
van Hinsbergen, D.J.J., Lippert, P.C., Li, S., Huang, W., Advokaat, E.L., Spakman, W., 2019. Reconstructing Greater India: Paleogeographic, kinematic, and geodynamic perspectives. Tectonophysics 760, 69–94.
van Hinsbergen, D.J.J., Schouten, T.L.A., 2021. Deciphering paleogeography from orogenic architecture: constructing orogens in a future supercontinent as thought experiment. Am. J. Sci. 321, 955–1031.
van Hinsbergen, D.J.J., Steinberger, B., Doubrovine, P.V., Gassmöller, R., 2011b. Acceleration and deceleration of India-Asia convergence since the Cretaceous: Roles of mantle plumes and continental collision. J. Geophys. Res. 116, B06101. https://doi.org/10.1029/2010JB008051.
van Hinsbergen, D.J.J., Torsvik, T., Schmid, S.M., Matenco, L., Maffione, M., Vissers, R. L.M., Gürer, D., Spakman, W., 2020. Orogenic architecture of the Mediterranean region and kinematic reconstruction of its tectonic evolution since the Triassic. Gondwana Res. 81, 79–229.
Verdel, C., van der Pluijm, B.A., Niemi, N., 2012. Variation of illite/muscovite 40 Ar/39 Ar age spectra during progressive low-grade metamorphism: an example from the US Cordillera. Contrib. Miner. Petrol. 164, 521–536.
Vogt, T., 1927. Sulitjelmafeltets geologi og petrografi. Norges Geologiske Undersokelse 121, 1–560 (in Norwegian, with English abstract).
Wajzer, M., Barber, A., Hidayat, S., 1991. Accretion, collision and strike-slip faulting: the Woyla Group as a key to the tectonic evolution of North Sumatra. J. SE Asian Earth Sci. 6, 447–461.
Wang, J.-G., Wu, F.-Y., Tan, X.-C., Liu, C.-Z., 2014. Magmatic evolution of the Western Myanmar Arc documented by U-Pb and Hf isotopes in detrital zircon. Tectonophysics 612–613, 97–105.
Weber, K., 1972. Notes on the determination of illite crystallinity. Neues Jahrbuch für Mineralogie, Monatshefte 267, 276.
Westerweel, J., Licht, A., Cogné, N., Roperch, P., Dupont-Nivet, G., Kay Thi, M., Swe, H. H., Huang, H., Win, Z., Wa Aung, D., 2020. Burma Terrane collision and northward indentation in the Eastern Himalayas recorded in the Eocene-Miocene Chindwin Basin (Myanmar). Tectonics 39.
Westerweel, J., Roperch, P., Licht, A., Dupont-Nivet, G., Win, Z., Poblete, F., Ruffet, G., Swe, H.H., Thi, M.K., Aung, D.W., 2019. Burma Terrane part of the Trans-Tethyan arc during collision with India according to palaeomagnetic data. Nat. Geosci. 12, 863–868.
Willis, K., Stern, R., Clauer, N., 1988. Age and geochemistry of Late Precambrian sediments of the Hammamat Series from the Northeastern Desert of Egypt. Precambr. Res. 42, 173–187.
Yang, L., Xiao, W., Julleh Jalalur Rahman, M., Windley, B.F., Schulmann, K., Ao, S., Chen, Z., Li, R., 2019. Provenance of the Cenozoic Bengal Basin sediments: Insights from U–Pb ages and Hf isotopes of detrital zircons. Geological Journal 54, 978-990.
Yao, W., Ding, L., Cai, F., Wang, H., Xu, Q., Zaw, T., 2017. Origin and tectonic evolution of upper Triassic Turbidites in the Indo-Burman ranges, West Myanmar. Tectonophysics 721, 90–105.
Zhang, X., Chung, S.-L., Lai, Y.-M., Ghani, A.A., Murtadha, S., Lee, H.-Y., Hsu, C.-C., 2019. A 6000-km-long Neo-Tethyan arc system with coherent magmatic flare-ups and lulls in South Asia. Geology 47, 573–576.
Zhang, X., Chung, S.-L., Tang, J.-T., Maulana, A., Mawaleda, M., Oo, T., Tien, C.-Y., Lee, H.-Y., 2020. Tracing Argoland in eastern Tethys and implications for India-Asia convergence. Geol. Soc. Am. Bull.
Zhang, J., Xiao, W., Windley, B.F., Cai, F., Sein, K., Naing, S., 2017. Early Cretaceous wedge extrusion in the Indo-Burma Range accretionary complex: implications for the Mesozoic subduction of Neotethys in SE Asia. Int. J. Earth Sci. 106, 1391–1408.
Zhang, J., Xiao, W., Windley, B.F., Wakabayashi, J., Cai, F., Sein, K., Wu, H., Naing, S., 2018. Multiple alternating forearc-and backarc-ward migration of magmatism in the Indo-Myanmar Orogenic Belt since the Jurassic: Documentation of the orogenic architecture of eastern Neotethys in SE Asia. Earth-Science Rev. 185, 704–731.